Biointerface Research in Applied Chemistry
Platinum Open Access Journal (ISSN: 2069-5837)

Review
Volume 12, Issue 3, 2022, 4261 - 4292
https://doi.org/10.33263/BRIAC123.42614292

Zinc Oxide Nanoparticles Synthesis Methods and its Effect on Morphology: A Review

Eric Kwabena Droepenu [1,2,*], Boon Siong Wee [1,*], Suk Fun Chin [1], Kuan Ying Kok [3], Muhammad Firdaus Maligan [1]

[1] Resource Chemistry Program, Faculty of Resource Science and Technology, Universiti Malaysia Sarawak 94300, Kota Samarahan, Sarawak, Malaysia
[2] Graduate School of Nuclear and Allied Sciences, University of Ghana, AE1, Kwabenya-Accra, Ghana
[3] Malaysian Nuclear Agency, Bangi, Kajang, 43000 Selangor, Malaysia
* Correspondence: swboon@unimas.my (B.S.W.); kobladodzie01@yahoo.com (E.K.D.);

Scopus Author ID 57194506096
Received: 28.06.2021; Revised: 1.08.2021; Accepted: 5.08.2021; Published: 14.08.2021

Abstract: Zinc oxide is an important material with numerous applications due to its unique properties. Due to their thermal and chemical stability are used in wide applications such as LEDs, sensors, catalysts, and photodetectors. Different chemical, physical, and biological methods have been adopted to achieve the intended result, as enumerated in many pieces of literature. Therefore, selecting an efficient synthesis process is essential, which is a key factor that significantly influences the efficacy of the synthesized nanocrystalline materials. The chemical synthesis of nanoparticles (NPs) via hydrothermal, solvothermal, and sol-gel routes is considered effective as high-quality crystalline structures are produced. Control of parameters of processes yields excellent morphological features of the synthesized samples. This review explored the different parameters of processes and their effect on the morphology of ZnO nanostructures via hydrothermal, solvothermal, and sol-gel techniques. Finally, some ZnO nanocomposites molecules are reviewed as per the dopant used and its effect on the sample compound synthesized.

Keywords: synthesis methods; nanostructures; nanomaterials; nanoparticles; zinc oxide; morphology.

1. Introduction

Zinc oxide is one example of transition metal oxides that exhibit unique electrical, optical and mechanical properties. Due to their unique properties, they have numerous applications in fields such as pharmaceuticals, electronics, consumer goods, optical and electrical devices, and environmental remediation [1-5]. The morphology of ZnO nanostructures has a significant role in their applications, according to Jin and Jin 2019 [6]. For instance, rod-like, sheet-like, and belt-like nanostructures are suitable for solar cells, light-emitting diodes, gas sensors, and biological probes. Interestingly, researchers focus on the morphology of nano ZnO to achieve their intended purpose in its applications. Controlling the size and shape of these nanostructures during synthesis is the major focus of the researcher.

Different synthesis techniques have been developed to be grouped into physical, chemical, and biogenic (green route). Physical techniques include pulsed laser deposition, magnetron sputtering, electrodeposition, and electron beam evaporation [7-11]. The chemical synthesis route comprises hydrothermal, solvothermal, sol-gel, chemical bath deposition, wet chemical process, spray pyrolysis, microemulsion, and precipitation methods [12-18]. Green

or biogenic synthesis of metal oxide nanomaterials is plant or microbe mediated, with the extracts being biocompatible and can serve as capping agents for stabilizing the NPs [19, 20]. Although chemical synthesis poses toxicity to the environment, pure desired crystals with high stability and high yield are produced [21].

ZnO nanostructures morphology and size of ZnO nanostructures can be modified when reaction conditions (precursor and their concentrations, temperature, solvent type, and surfactants) in a particular synthesis route are controlled [22]. It was reported that, although different treatment methods and surfactants were used in the synthesis of ZnO nanostructures, similar flower-like structures were obtained using the same precursor (zinc acetate dihydrate) [23-24]. The use of surfactants (HMT and PEG 400) and annealing the synthesized ZnO nanocrystalline powder at 500 ^{o}C by Rocha *et al*. [23] resulted in the particle to record crystallite size of 30 nm as against free surfactant and without extra heat at a crystallite size of 7-8 nm. In another study by Vahidi *et al*. [25], ZnO NPs of different crystallite sizes (51, 60, and 61 nm) but similar aggregated spherical shaped particles were obtained using *Pelargonum zonale* leaf extract and zinc nitrate as a precursor under different heating conditions (conventional heating, autoclave, and microwave irradiation). However, samples from the conventional heating process recorded the highest antibacterial effect of the bacterial strains used for the study. When this study was compared to that of Satheshkumar *et al*. [26], although the same morphology of aggregated spherical shaped particles was produced from the conventional heating process, the crystallite size was far below (1.62-1.88 nm) that of Vahidi *et al*. These variations may be attributed to different conditions such as the concentrations of the precursor and extracts used as well as the reaction conditions under which each sample was prepared. These reports indicate that variation of synthesis parameters could affect the morphology of crystals produced.

Literature suggests that different techniques are being developed for a suitable and easy means to achieve desired properties of these nanostructures. However, it was reported that wet techniques of synthesizing metal oxide nanomaterials usually produce impure particles with larger particle sizes [27]. These limitations result from the complexity of the chemical reactions during the growth and nucleation stages of the reaction mechanism, which makes it impossible for repeatability. Therefore, selecting an efficient synthesis process is essential, which is a key factor that significantly influences the efficacy of the synthesized nanocrystalline materials. This review critically examines the current development of appropriate reaction conditions that could be employed in four chemical synthesis methods (hydrothermal, solvothermal (microwave-assisted), sol-gel and hybrids) to achieve the desired features of zinc oxide nanoparticles needed for its specific application.

2. ZnO Nanoparticles Synthesis by Hydrothermal Route

This route of synthesizing ZnO nanoparticles involves using high heat and pressure (100-1000 °C and 1-10,000 atm) with water as a solvent in an autoclave (Figure 1). Although good quality crystals are produced, high energy consumption in some cases coupled with expensive autoclaves is some disadvantages to this technique. The heating method may be conventional or microwave, with each having its advantages and disadvantages. Other parameters such as the type of reactant, alkaline source, doping material, surfactant, or reaction conditions (calcination temperature and reaction time) determine the characteristics of nano ZnO synthesized. Conventional heating employs the principle of conduction and convection within the reaction medium resulting in the non-uniformity of heat to the molecules. Molecules

are subjected to heat sources via two modes; First, where there is direct contact with the reacting molecules and the heat source element. And secondly, the heating element may be in contact with the containing vessel of the reaction mixture in the case of a heating mantle. The former may result in contaminations by the heating element in direct contact with the mixture. However, the latter is mostly preferred. This effect subsequently affects the nature and quality of samples synthesized. In furtherance to this, there is a high loss of heat as a result of the long duration of the heating process. Also, 'wall effect' is a phenomenon where the maximum temperature is experienced at the reaction vessel walls, leading to the heterogeneity of the obtained products. However, microwave irradiation is characterized by a short heating time with the heating directed to the molecules (precursor and solvent) by microwaves' energy, thereby providing intense friction and collision between the molecules, which accelerates the nucleation process [28]. Microwave heating ensures the synthesis of pure samples as there is uniformity in the heating of the molecules [29, 30]. For instance, the capability of solvent molecules to be irradiated at a given temperature and frequency to heat energy known as loss factor (loss factor of deionized water is 0.123) renders microwave heating more efficient in the hydrothermal method of synthesis [31]. However, impurities in the solvent decrease the penetration depth, according to Kim *et al*. [32]. These factors indicate that reaction molecules have acquired an electric dipole moment in proportion to the applied electric field.

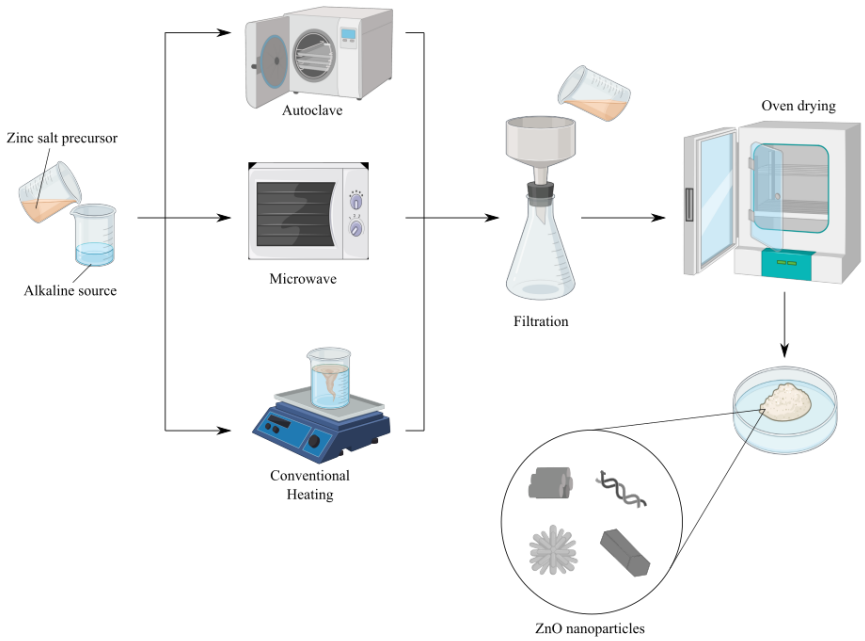

Figure 1. Overview of the hydrothermal method to synthesize ZnO nanoparticles.

ZnO nanocrystals were synthesized using autoclave mode of heating at temperatures between 100-150 ^{o}C for 1-5 hours by Vellakkat *et al*. [33]. The study reported that variation of reaction temperature and time produced diverse morphologies (flower-like, rod-like, and spherical granular). The study also reported that an increase in temperature time decreased the crystallite size (46.19, 41.66, and 34.74 nm), whereas an increase in reaction time increased the size (44.76, 53.51, and 78.21 nm). Meanwhile, high purity hexagonal wurtzite ZnO nanocrystals were produced from microwave-assisted hydrothermal technique by Ming *et al*. [34]. From their study, a mixture of zinc nitrate, potassium sodium citrate, and sodium hydroxide solutions was irradiated in a microwave oven (650 W, 2.45 GHz) for 20 minutes at 90 ^{o}C. High resolution of the spherical surface features of the particles revealed numerous

interconnected nanosheets, which were displayed as microflower in the TEM analysis. In addition, the synthesized sample exhibited a high photocatalytic performance for Rhodamine B degradation due to its smaller band gap.

According to Suwanboon *et al*. [35], the type of precipitating agent (alkaline source) used influences the morphology of the ZnO nanocrystals produced. In their study, hexagonal columnar structures changed to hexagonal platelet structures with crystallite size (55.8-57.8 nm) as the molar concentration of LiOH increased from 0 to 2 when the reaction mixture was autoclaved at 180 ^{o}C for 15. However, NaOH produced rod-like structures (Figure 2a) with crystallite size (46.7-48.0 nm) under the same conditions. The study concluded that, whereas hexagonal ZnO platelets (Figure 2b) showed better photocatalytic efficiency to methyl blue, the rod-like structures exhibited better inhibitory activity against *Staphylococcus aureus*.

The effect of surfactants on the morphology of ZnO nanocrystals was investigated by Zhu *et al*. [36]. They reported that an increase in the concentration of CTAB (0.03-0.1 M) saw plate-like nanostructures aggregated to form flower-like structures (Figure 2c). A further increase in CTAB to 0.3 M collapsed the flower-like structures. The synthesis conditions were reaction time of 3 hours, autoclave temperature of 150 ^{o}C for 16 hours, and calcination temperature of 500 ^{o}C for 2 hours. These flower-like nanostructures have been investigated as suitable materials for Sulphur dioxide gas detection [37] and ethanol sensing [36].

In other studies, the effects of reactants on the morphological structures of ZnO nanostructures were investigated. Perillo *et al*. [38] and Alver *et al*. [39] employed different zinc salt precursors [$Zn(CH_3COO)_2{\cdot}2H_2O$; $ZnCl_2$ and $Zn(NO_3)_2{\cdot}6H_2O$] and hexamethylenetetramine (HMTA) at 90 °C for 6 hours on a magnetic stirrer and 140 ^{o}C for 4 hours in an autoclave respectively. HMTA acted as a pH buffer to release the OH^- from the reaction mixture. Perillo *et al.* recorded hexagonal nano-rods with crystallite size (40-46 nm), particle length, and diameter (400 nm-6.5 µm and 73-300 nm) for all the precursors. Although Alver *et al.* also produced hexagonal rod-like nanostructures from zinc acetate and zinc nitrate precursors, zinc chloride produced hexagonal rod-like and plate-like structures (impurity). This impurity confirms the assertion made by Wojnarowicz *et al*. [27] that zinc chloride produces a stable by-product (simonkolleite), which is considered an impurity during the synthesis of ZnO.

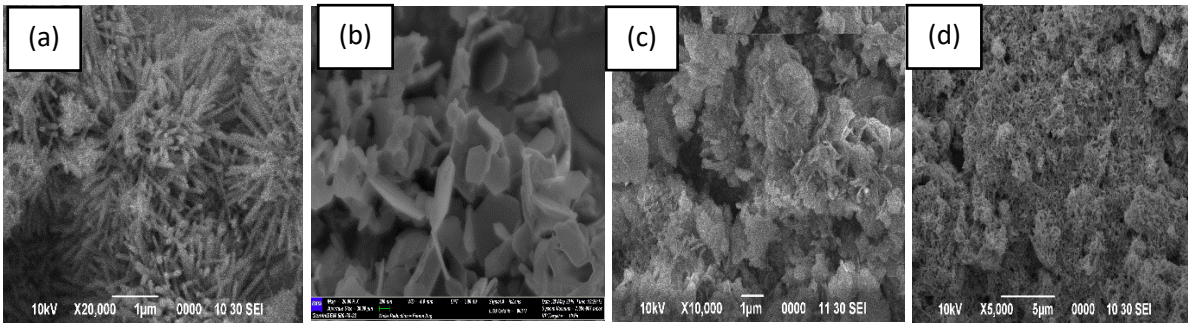

Figure 2. ZnO morphologies:(**a**) rod-like; (**b**) hexagonal platelets; (**c**) flower-like; (**d**) wire-like nanostructures.

Amin *et al*. [40] also investigated the effect of pH, precursor concentration, growth time, and temperature on the morphology of ZnO nanostructures. They reported that tetrapod-like, flower-like, and urchin-like structures were obtained when the pH of the reaction mixture was from 8-12.5. However, as the pH was lowered from 8 to 4.6, rod-like structures eroded gradually to wire-like nanostructures (Figure 2d). Meanwhile, when the concentration of the precursor $Zn(NO_3)_2{\cdot}6H_2O$, was also decreased from 400-25 mM, the micro-rods observed at pH 8 gradually thinned out to wire-like structures with a diameter (< 100 nm) and length (1.2

µm). The average length of the rod-like structures produced was directly proportional to growth duration. The first 6 hours increased the length from 500 nm to 1.8 µm until the final length increased to 2.2 µm at the 10th hour. There was no further increase in length after the 10 hours of duration. They also reported that the aspect ratio of the synthesized rod-like structures increased with increasing temperature from 50 ^{o}C to 95 ^{o}C beyond which there was no change. Similarly, rod-like nanostructures were reduced to thin-film macrostructures when the precursor concentration was increased from 10 mM to 500 mM [41]. Table 1.0 illustrates other literature on hydrothermal synthesis using microwave-assisted and conventional approaches in ZnO nanostructures synthesis and their applications.

2.1. ZnO nanoparticles synthesis by the solvothermal route.

The solvothermal technique is a widely used technique that usually uses non-aqueous solvents under controlled temperature and pressure higher than atmospheric pressure [42]. This technique requires a simple setup (Figure 3), less expensive equipment, relatively low synthesis temperature to yield a large area of deposition [43]. The technique also allows the microstructural control of the particles produced and the dispersity of ZnO NPs [44]. Despite these advantages, some of the solvents used are very costly and are very toxic to the environment.

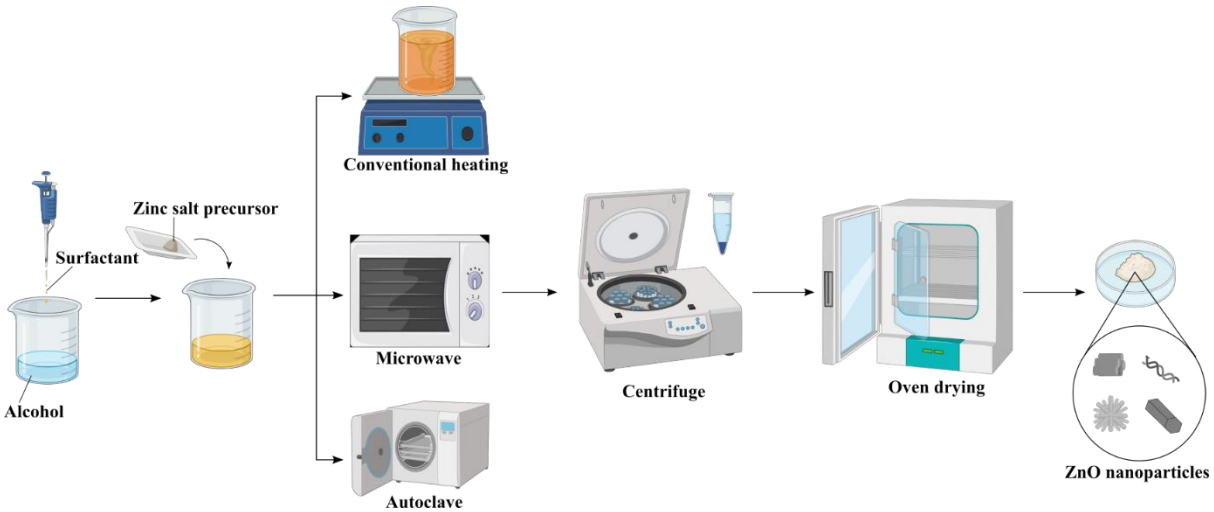

Figure 3. Overview of the solvothermal method to synthesize ZnO nanoparticles.

According to Šarić *et al*. [45], properties of the non-polar solvents enable the reaction mechanism and particle growth to be controlled easily as moisture to the system is eliminated. The intermediate species from the non-polar solvents used in this technique offer better characterization when analyzed with NMR spectroscopy compared to the aqueous system [46. These non-polar solvents can serve as surfactants. The type of non-polar solvent and its intermediate species formed during the synthesis process could affect the crystal growth as selectivity to the different facets of the ZnO crystal is possible [47].

In most solvothermal syntheses, ethanol and methanol (alcohol) are the most common solvents used due to their availability and cost. Other solvents, as well as surfactants used according to literature, including oleic acid, gluconic acid, tween 80 [48], ethylene glycol [49-51], triethanolamine, TEA [43]. Surfactants are amphiphilic molecules classified as anionic, nonionic, cationic, or amphoteric in terms of charge present in the hydrophilic portion of the molecule after dissolution in an aqueous solution. They usually form water-in-oil micro-emulsions which may be of two or three categories; the first metal complex dissolved in the

water pools, another metal salt complex, and the reducing agent. An example is the mixture of both platinum and palladium salts in the presence of sodium bis (2-ethylhexyl) sulfosuccinate (AOT) as surfactant and hydrazine as a reducing agent [52]. The surfactants tend to restrict the growth of the particles as the size of the emulsion, therefore, tend to determine the particle size. Šarić *et al*. [45] established that increase in the mole ratio of the surfactant and type of alcohol use increases the particle size. According to a review by Wojnarowicz *et al*. [27], surfactants such as Triton X100, polyethylene glycol 400 (PEG-400), polyvinylpyrrolidone (PVP) produces rod-like nanostructures [53], polyvinyl alcohol (PVA) results in the production of flake-like nanostructures [54], whiles polyvinylpyrrolidone (PVP) and cetyltrimethylammonium-bromide (CTAB) produces flower-like nanostructures [55].

The reaction kinetics of the molecules are mainly governed by the transport of species through the heat transfer within the system. As indicated previously, thermal decomposition of reacting molecules is efficient when microwave irradiation is used compared to conventional heating. One microstructural property of ZnO NPs that influences their application is the agglomeration of the synthesized crystals. Literature has reported that Diethanolamine (DEA) and Triethanolamine (TEA) are suitable solvents used as polymerization and stabilization agents in controlling the morphology of ZnO structures by the aggregation of primary nanoparticles [43,56]. In a study by Saric *et al*. [45], Triethanolamine (TEA) was investigated to have an impact on the growth of particles. The result established that TEA acted as both a suppressor and modifier of the particles formed at a reaction temperature of 170 ^{o}C. Furthermore, the growth and aggregation of the particles depended on the mole concentration ratio of the zinc precursor and TEA.

In other to develop the morphology of ZnO NPs to suit a particular application, Idiawati *et al*. [57] demonstrated the effect of growth time using a two-stage approach to grow ZnO nano-rods on Indium Tin Oxide (ITO) substrate. The first reaction stage (seed layer formation) employed zinc acetate dihydrate and Monoethanolamine (MEA) reaction at 70 °C for 2 hours. Then follows the growth stage where zinc nitrate tetrahydrate [$Zn(NO_3).4H_2O$], Hexamethylenetetramine [HMT], and ITO were reacted at 90 °C with the growth-time varied at 4, 6, and 9 hours for each concentration. The as-prepared ZnO nanorods gave the crystallite size, nanorod length, and diameter to be 44-51 nm, 570-1280 nm, and 138-236 nm, respectively. It has been proven that these rod-like nanostructures are showed resistance to wood decay fungus [58].

Nevertheless, Ming *et al*. [34] investigated the effect of different zinc salts (zinc sulfate, zinc nitrate, and zinc acetate) on Rhodamine B dye's morphology and photocatalytic property. The microwave operating conditions (650 W, 2.45 GHz) produced microsphere structures covered with nanosheets and nanoparticles (nitrate and sulfate zinc) and microflower structures covered with nanosheets (zinc acetate). Nitrate-ZnO sample exhibited the best photocatalytic degradation of 93.63% after 120 minutes compared to acetate-ZnO and sulphate-ZnO samples with percentage degradation of 82.35% and 64.66%, respectively. Other studies carried out using this route but with different conditions are illustrated in Table 2.0.

2.2. ZnO nanoparticles synthesis by sol-gel route.

Sol-gel as a chemical technique in metal oxide nanoparticle synthesis was a technology used to fabricate glass and ceramic materials some four decades ago, as reported by Dimitriev *et al*. [59]. The method is made up of aqueous and non-aqueous processes involving water and organic solvents. Aqueous sol-gel chemistry converts the precursor (mostly inorganic metal

salt or metal alkoxides) into inorganic solid by virtue of the water molecules. On the other hand, non-aqueous sol-gel chemistry transforms the precursor (usually metal acetylacetonates and acetates, organometallic compounds, metal alkoxides, inorganic metal salts) via thermal decomposition. Sol-gel was adopted because of its considerable use of reduced temperature, which was economical compared to physical methods. This technique also offers the desired rate of thermal stability, good flexibility of crystal formation that is reproducible, better control of the particle size and shape to suit a wide range of applications, and relatively inexpensive apparatus set-up [60, 61]. Devoid these advantages, there are a few fundamental problems regarding the aqueous process, according to Livage *et al*. [62]. First, many reaction parameters (pH, precursor concentration, temperature, method of mixing, oxidation rate, hydrolysis, and condensation) need careful control to achieve the desired result. Also, the synthesized sample is generally amorphous, which needs the right annealing temperature to get the required crystalline structure. However, the non-aqueous process tends to overcome some of these major limitations of the aqueous process.

Sol-gel employs either a chemical solution (sol) or colloidal particles to produce an integrated network (gel) involving aqueous or organic solvent. The process involves various steps, including hydrolysis and polycondensation, gelation, aging, drying, and crystallization, as illustrated in Figure 4.

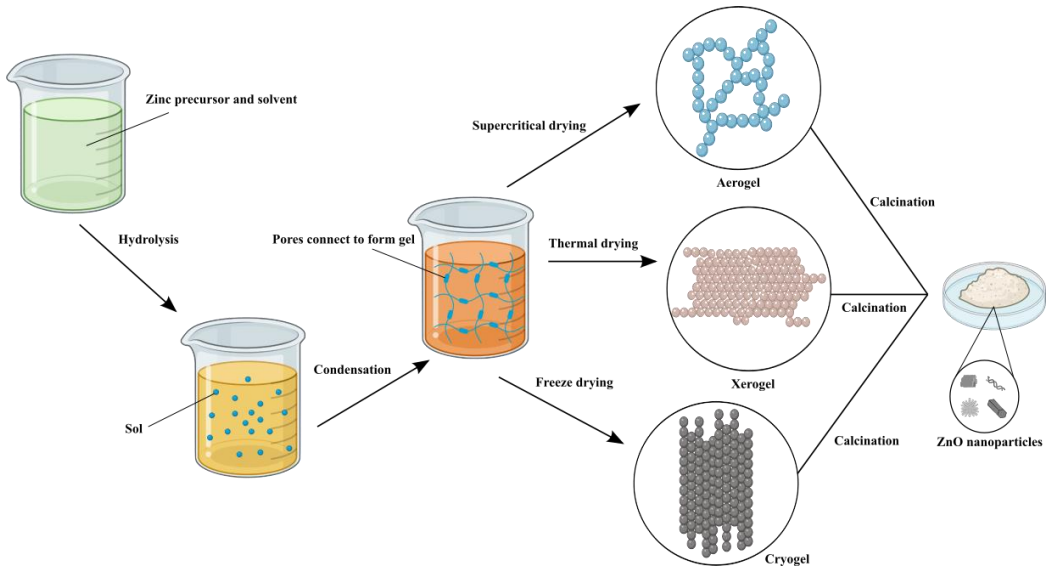

Figure 4. Overview of the sol-gel processes to synthesize ZnO nanoparticles.

Oxygen produced by the reaction solvent (water or alcohol) aids in forming the metal oxide in the hydrolysis stage. Alternatively, the use of an acid or alkaline source could also aid the hydrolysis of the precursor used. After the hydrolysis stage, the solvent condenses to form a colloidal mixture (gel), which yields hydroxyl (-OH) or oxo (-O) species to connect the metal molecules. The gelling process continues through the third stage until it is subjected to the type of drying, as illustrated in Figure 4. The type of drying process adopted affects the structure of the gel formed. Also, the nature of nanoparticles to be formed also depends on the drying process and relative humidity. For instance, nano-films may require low humidity for the stability of the sample formed. As already stated, calcination of the sample also influences the nature of the sample formed in terms of morphology [64, 65].

Shaikh and Ravangave [66] used the sol-gel method to synthesize nanorod structures with crystallite size in the range of 33-43 nm when zinc acetate and sodium hydroxide were

used as starting materials. The reaction time was varied between 2-8 hours, after which the as-prepared samples were calcined at 100 ^{o}C for 2 hours. Hasnidawani et al. [67] synthesized rod-like nanostructures with an average particle size of 81-85 nm with similar starting materials. Differences could be attributed to calcination and the longer reaction time employed by Shaikh and Ravangave.

According to Iwamura *et al*. [68], reaction time and purity of the nanomaterial can be enhanced with the use of the microwave-assisted sol-gel technique. Irradiation of zinc acetate dihydrate and N, N-dimethylacetoamide (DMAc) with a temperature of 64-118 °C for 1.5-4.0 min duration yielded spherical nanocrystalline structures with a particle size of 312-509 nm. However, an increase in time to 6 min altered the morphology to nanowires of length and diameter, 1334 and 127 nm, respectively. Also, the good and quality yield of cubic octamethylsilsesquioxane was synthesized using microwave-assisted technique [69].

The type of reagent used in sol-gel synthesis also influences the morphology as well as the optical properties of the synthesized samples. According to Vanaja and Rao [70], potassium and sodium hydroxide were used as precipitating agents on the precursor, zinc nitrate. Potassium hydroxide produced a smaller crystallite size (21.59 nm) of ZnO as compared to 36.89 nm when sodium hydroxide was used. Both agents produced irregular spherical-shaped structures with sizes 17-25 nm and 30-50 nm for KOH and NaOH, respectively.

Apart from the solvent controlling the reaction mechanism in non-aqueous sol-gel processes, surfactants can also be used in the presence of the precursor in the transformation process, thereby acting as stabilizing ligands at temperature ranges of 250-350 ^{o}C. The surfactant's ability to select the specific crystal face during the growth stage enables the control of the morphology and agglomeration as well as the surface properties of the nanoparticles. However, surface-adsorbed surfactant compromises the gas sensing effect or catalysis of some nanomaterials as well as their toxicity [71]. Thorn-like ZnO nanostructures were synthesized through the sol-gel method by Khan *et al*. [72], when zinc acetate, sodium hydroxide, and cetyltrimethylammonium bromide (CTAB) was reacted under different stirring conditions (500, 1000, 1500, and 2000 rpm) for half an hour. Although other nanostructures such as nanoflowers, nanorods, nanowhiskers, nanobelts, nanotubes, nanorings, and nanocolumns were also identified, the thorn-like structures (Figure 5) were dominant with size determined at < 50 nm by TEM analysis.

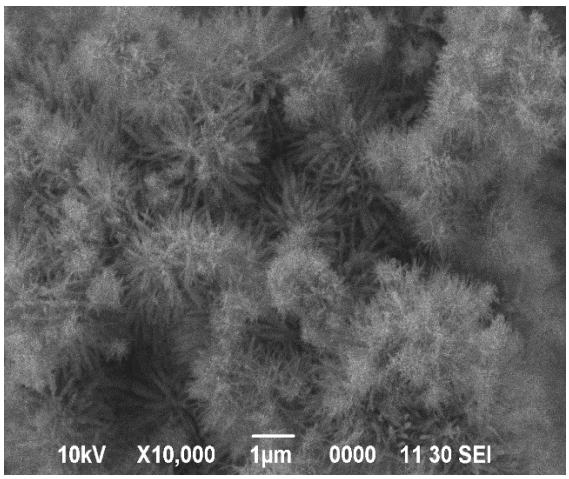

Figure 5. Thorn-like ZnO nanostructures.

Brintha and Ajitha [73] compared the morphological differences when ZnO nanostructures were prepared using sol-gel, hydrothermal and aqueous solution techniques.

Although sol-gel employed high annealing temperature of 450 ^{o}C for 6 hours, the other techniques had their reaction temperatures between 80-100 ^{o}C for 6 hours. Hydrothermal and sol-gel techniques produced spherical and flower-like structures with 14 nm and 18 nm crystallite, respectively. On the other hand, the aqueous solution technique recorded a mixture of the two structures with a crystallite size of 13 nm. Results from this study were similar to that of [74] when ZnO was doped with Ni and Al in a sol-gel process. Other studies carried out using the sol-gel method of synthesis with different conditions and useful application of the as-prepared samples are illustrated in Table 3.0.

2.3. ZnO hybrid/composite synthesis route.

The intent of producing suitable changes in electrical, optical, and magnetic properties of metal oxide nanomaterials for their intended practical purposes is through the use of some selected elements in the periodic table (Group I, II, III, transition metals, metalloids, non-metals, and lanthanides) as doping materials [75]. Since these transition elements are semiconductors, creating defects in the lattice of these semiconductors or forming hybrid materials with their required properties helps make the fabricated composite material an effective photocatalyst. Elements that are suitable as dopants in ZnO nanostructures should have a small ionic radius as that of Zn (0.74 Å). This enables the ions to easily migrate over the crystal to occupy the interstitial positions, thereby affecting the nanocomposite compound's structural, morphological, and optical properties. According to Yousefi *et al*. [76], Li-doped ZnO showed better crystal quality than Na and K-doped ZnO as well as the undoped ZnO. It was also evident that, when alkaline earth metals (Mg^{2+}, Ca^{2+}, Sr^{2+}, and Ba^{2+}) was used as a dopant in a co-precipitation technique by Hameed *et al*. [77], XRD patterns of Mg and Ca-doped-ZnO showed no addition phase due to their ionic radii (0.66 Å & 0.99 Å) been close to that of Zn where the others were far above (1.13 Å for Sr^{2+} and 1.35 Å for Ba^{2+}). The doped samples showed better enhancement in the crystalline nature as compared to the undoped sample.

Transition metal (TM) doped ZnO nanostructures are explored due to the magnetic and electronic properties they exhibit as a result of the electron spins in the 3d-orbital. Composite nanostructures synthesized from these species have better applications in electrical, electronics, and magnetic devices as compared to the bulk. The ionic radius of TMs was established to be one of the determining parameters for producing a very pure doped nanocrystalline structure. Zak *et al*. [78] identified Ni, Mn, and Co-doped ZnO to show a decreased particle size compared to the undoped. This result was attributed to the similar ionic radius of the dopants, Ni (0.69 Å), Co (0.745 Å), and Mn (0.46 Å) to Zn, where their lattice strain was replaced by Zn in the lattice structure.

From a study by Kaur *et al*. [79], Gd-doped-ZnO exhibited a paramagnetic behavior with a weak ferromagnetic component at low Gd-doping compared to the undoped. The doped sample was synthesized using zinc acetate dihydrate and gadolinium nitrate in 2-methoxy ethanol as solvent at 60 ^{o}C for 2 h. After adding monoethanolamine, the sol was aged 24 h at room temperature, dried at 500 ^{o}C for 1 h, and finally annealed at 500 ^{o}C for another 1 h. Results from this study showed the formation of rod-like nanostructures with an average crystallite size of 25-37 nm. These hybrid nanostructures can be synthesized using different techniques. Table 4.0 illustrates doped-ZnO nanostructures synthesized by different techniques.

Table 1. Characteristics of ZnO nanostructures synthesized via different hydrothermal routes.

Method of synthesis	Precursor/Reactant	Synthesis condition	Properties	Applications	Reference
Microwave-assisted without extra heat treatment	$Zn(Ac)_2 \cdot 2H_2O$, NH_4OH/NaOH, AOT	Reaction time: 10 min; Autoclave temp: 80, 100, 120 or 140 °C for 5, 10, 20 min; Microwave power: 300, 600 and 1200 W; Drying time: 65 °C for 3 h.	Hexagonal prism-like structures; Particle size: 200-300 nm		[80]
Microwave-assisted + heat treatment	$Zn(Ac)_2 \cdot 2H_2O$, N_2H_4, $Zn(NO_3)_2 \cdot 6H_2O$, NaOH, NH_3	Irradiation: 15/10 min 510/680 W; Drying: 100 °C 2 h; Irradiation: 15 min 150 W; Drying: 100 °C 2 h; Calcination temp: 600 °C 3 h	Needle-like, Flower-like, Spherical: Particle diameter: 50-150 nm		[81]
Microwave-assisted without extra heat treatment	$Zn(Ac)_2 \cdot 2H_2O$, NaOH (solvent = water/ethyl alcohol; 50/50 v/v & 100/0 v/v)	Reaction temp: 100 °C & 140 °C for 45 and 60 min; Microwave power: 800 W; Drying temp: 80 °C overnight; pH = 10	Plate-like, rounded plate-like, brush-like, and flower-like; Band gap: 3.17-3.24 eV; Surface area: 8.46-10.70 m^2/g	Photocatalyst against Rhodamine-B	[82]
Microwave-assisted without extra heat treatment	$Zn(NO_3)_2$, NaOH	pH = 8.3; Microwave irradiation: 1-5 min; Drying temp: 70 °C	Rod-like, flower-like; Particle size (diameter): 100-200 nm; Hydrodynamic size (DLS): 135-361 nm	Bio-imaging and drug (Quercetin) delivery	[83]
Microwave-assisted without extra heat treatment	$ZnCl_2$, NaOH, CTAB, Pluronic F127	reaction temp: 50 °C for 90 min; Microwave power: 2.45 GHz; 130 W for 5 min; Drying temp: 60 °C for 24 h	Cone-like (surfactant free & Pluronic F127), Plate-like (CTAB); Surface area: 15.5-24.8 m^2/g; Crystallite size: 19.6-21.0 nm; Particle size: 92.8 nm; 58.1 nm (CTAB); 80.2 nm (Pluronic F127); Band gap: 3.36 eV (free surfactant and CTAB); 3.34 eV (Pluronic F127)	Photocatalyst in the degradation of methyl blue (MB)	[84]
Microwave-assisted without extra heating	***ACF Fabric Preparation***: ACF + HNO_3 ***Growth of ZnO***: Zn(Ac) + NH_4OH, on ACF fabric	Reaction time: 1 h; Drying temp: 50 °C (oven), 100 °C for 3 h (furnace) Reaction time: 3 h Microwave power: 1120W, 2450 MHz for 30 min x 3 steps; Drying temp: 50 °C for 24 h; pH = 10-11	Rod-like structures	Removal of tetracycline	[85]
Microwave-assisted without extra heating	$Zn(Ac)_2 \cdot 2H_2O$, TEOA, BTCA, KOH	Microwave power: 2.45 GHz, 800 W, 150°C, 30 min; Drying temp: 100 °C; pH = 12/13	Dumb-bell (pH 8), Spherical (pH 9) Hexagonal bi-pyramidal (pH 10); Surface area: 35, 15, 25 m^2/g (Dumb-bell, spherical, hexagonal bi-pyramidal); Particle size: 195, 430, 60 nm (Dumb-bell, spherical, hexagonal bi-pyramidal)	Photoelectrode	[86]

Method of synthesis	Precursor/Reactant	Synthesis condition	Properties	Applications	Reference
Microwave-assisted with extra heating	***ZnO nanorods synthesis*** $Zn(Ac)_2{\cdot}2H_2O$, NaOH (Mole ratio: Zn^{2+}: OH^- (1: 0,3,6,9,12,15) ***ZnO photoanode synthesis*** ZnO, PEG, C_2H_5OH	Microwave power: 450 W, 5 min; Drying temp: 80 °C for 24 h Reaction time: 1.5 h; Drying temp: 80 °C for 30 min; Calcination temp: 450 °C for 1.5 h	Plate-like, flower-like structures; Energy band gap: 3.201-3.217 eV	Photoanode, Photocatalyst in the degradation of methyl blue (MB)	[87]
Microwave-assisted without extra heating	$Zn(NO_3)_2{\cdot}6H_2O$, NaOH	Microwave power: 70-100 W, 100-240 °C, 3-7 min, 9-49 bars; Reactor parameters: 120-200 °C, 30 min, 1-14 bars; Drying temp: 50 °C for 2 h	Particle size: 20-250 nm; Crystallite size: 22-30 nm; Particle size: 30-400 nm; Crystallite size: 30-32 nm		[88]
Microwave-assisted without extra heating	$Zn(NO_3)_2{\cdot}6H_2O$, NaOH, Gum Arabic	Microwave power I: 350 W for 2 min; Microwave power II: 350 W for 2, 4, 6 & 10 min; Drying temp: 80 °C; pH = 10	Spherical; Crystallite size: 25 nm (2 min); Particle size (DLS): 160-180 nm (2-6 min); 225 nm (10 min); Particle size (FESEM): 20-40 nm (non-aggregate); 150-200 nm (aggregates)		[89]
Microwave-assisted without extra heating	***Seed layer preparation***: $Zn(Ac)_2{\cdot}2H_2O$, C_3H_8O ***Growth of ZnO nanorod***: Substrate, $Zn(NO_3)_2{\cdot}6H_2O$, HMTA	Annealing temp: 300 °C for 30 min (3x); Microwave power I: 900 W for 2 min; < 50 PSI; Microwave power II: 100 & 1600 W, 80 °C, for 5 & 15 min	Rod-like and rod-like thin film structures; Nanorod diameter: 40-50 nm (one step), 600 nm (two-stem); Crystallite size: 1-10 µm (one step), 200 nm (two step)	Electronic switch	[90]
Microwave-assisted without extra heating	$Zn(NO_3)_2{\cdot}6H_2O$, NaOH (4, 5 & 6 mmol of NaOH)	Microwave power: 110 °C for 1 h; Drying temp: 80 °C for 24 h	Star-like and chrysanthemum flower-like structures; Energy band gap: 3.21, 3.22 & 3.24 eV; Crystallite size: 26, 24, 21 nm respectively.	Photocatalyst for reduction of chromium(VI)	[91]
Microwave-assisted without extra heating	$Zn(Ac)_2{\cdot}2H_2O$, NaOH	Reaction temp: 75 °C for 2 h; Autoclave temp: 100, 125, 150, 175 & 200 °C for 8, 12, 16, 20, & 24 h; Drying temp: 75 °C for 6 h	Spherical shape (8-24 h), Spherical & rod-like (100-200 °C); Crystallite size: 31-38 nm (8-24 h); 27-35 nm (100-200 °C); Particle size (HR-TEM): 30-40 nm; Energy band gap: 2.90-3.78 eV		[92]
Microwave-assisted without extra heating	$Zn(NO_3)_2{\cdot}6H_2O$, NaOH	Microwave power: 2.45 GHz, 1000 W, 10 min; Drying temp: 60 °C overnight; pH = 10	Spindle-like; Crystallite size: 21 nm; Surface area: 11.06 m^2/g (ZnO)	Antidiabetic & antibacterial inhibitor	[93]
Microwave-assisted without extra heating	$Zn(NO_3)_2$, NaOH	Irradiation time: 15 min; Drying temp: 60 °C for 24 h; pH = 10	Spherical shape; Crystallite size: 15.5 nm (ZnO)	Antidiabetic activity	[94]
Microwave-assisted without extra heating	***Seed layer preparation***: $Zn(Ac)_2{\cdot}2H_2O$, C_3H_8O	Annealing temp: 310 °C for 60 min Microwave Power: 2.45 GHz, 105 °C for 5, 10 & 15 min; Drying: N_2 gas	Rod-like; Particle diameter & length: 26-32 nm & 440 nm (75 mM), 35–39 nm &		[95]

Method of synthesis	Precursor/Reactant	Synthesis condition	Properties	Applications	Reference
	Precursor growth: $Zn(NO_3)_2{\cdot}6H_2O$ (75 mM, 0.1 M, 0.2 M), $C_6H_{12}N_4$		600 nm (1.0 M), 78–84 nm & 1.5 µm (2.0 M) 22-26 nm & 430 nm (0.1 M @ 5 min), 35-40 nm & 60 nm (0.1 M @ 10 min), 35-39 nm & 605 nm (0.1 M @ 15 min)		
Microwave-assisted without extra heating	$Zn(Ac)_2{\cdot}2H_2O$, NaOH	Microwave Power: 2450 MHz, 700 W, 6 min; Drying temp: 60 °C for 4 h; pH = 6, 8, & 10	Irregular sheet-like (pH 6), Agglomerated uniform microstructures (pH 8 & 10); Particle size: ~100 nm (pH 8 & 10)	Antibacterial activity	[96]
Microwave-assisted without extra heating	***Seed layer preparation***: Si, ZnO deposit by RF magnetron sputtering ***Precursor growth***: $Zn(Ac)_2{\cdot}2H_2O$ (0.01~0.04 mol/L), $C_6H_{12}N_4$	Sputtering parameters: 100 W for 100 s, < 7×10^{-4} Pa and 1.0 Pa Microwave Power: 60-110 ºC, 5-40 min	Rod-like; Particle size (TEM): 90 nm		[97]
Microwave-assisted without extra heating	***Synthesis of 1-carboxy4-methylpyridin-1-ium*** C_6H_7N, $C_2H_3ClO_2$ ***Synthesis of Dye; {4-[(E)-2-(furan-2-yl) ethenyl]pyridin-1-ium-1-yl}acetate*** $C_6H_7NO_2$, $C_5H_5O_2$, $C_5H_4O_2$, C_2H_5OH, C_5H_5N ***ZnO synthesis*** $Zn(Ac)_2{\cdot}2H_2O$, Dye (1% & 3%), NaOH	Reaction time: 2 h; Refluxing temp: 70 ºC for 6 h; Microwave power: 20 min; Drying temp: 60 ºC for 8 h	Hexagonal wurtzite structure; Crystallite size: 30.6 nm (uncapped); 22.9 nm (3% dye-capped); Energy band gap: 3.6 eV	Bactericidal agent	[98]
Microwave-assisted without extra heating	$Zn(Ac)_2{\cdot}2H_2O$, TRIS (20%)	Microwave power: 300 W for 3 min; Drying temp: 80 °C overnight	Spherical; Energy band gap: 3.49 eV	Antifungal agent	[99]
Microwave-assisted without extra heating	$Zn(Ac)_2{\cdot}2H_2O$, Phthalic acid (PA)/ Isophthalic acid (IPA)/ Terephthalic acid (TPA)	Microwave power: 2.45 GHz, 800 W, 150 °C for 30 min; Drying temp: 100 °C for 12 h; pH = 7, 10 & 12	Platelet shape (SDA), star-like (TPA), rod-like (IPA), plate-like (PA); Particle size: 50-500 nm (free SDA), 100-150 nm (presence of SDA)		[100]
Microwave assisted with extra heating	$Zn(NO_3)_2{\cdot}6H_2O$, NaOH (1:15 molar ratio), PEG	Microwave power: 2.45 GHz, 320 & 480 W for 5 s & 15 s; Drying temp: 80 °C for 24 h; Calcination temp: 450 °C for 1 h	Needle-like (320 W), Rod-like (480 W); Particle size (PEG free/PEG): < 500 nm/ 300 nm length (320 W), 2 µm/3 µm length (480 W); Energy band gap: 3.24 Ev (PEG free), 3.10-3.23 eV (PEG)	Photocatalyst in the degradation of methyl blue (MB)	[101]
Microwave-assisted with extra heating	$NaC_{12}H_{25}SO_4$, C_3H_8O, NH_3, $Zn(Ac)_2{\cdot}2H_2O$	Reaction temp: 80 °C for 2 h; Microwave power: 2.45 GHz, 100-800	Fake-like (0.12 W/g), spherical (0.12 & 0.56 W/g); Crystallite size: 38.84 nm	Photocatalyst in the degradation of phenol	[102]

Method of synthesis	Precursor/Reactant	Synthesis condition	Properties	Applications	Reference
		W for 2 h, 0.12, 0.37 and 0.56 W/g; Calcination temp: 550 °C for 3 h	(0.12 W/g), 34.52 nm (0.37 W/g), 31.08 nm (0.56 W/g); Energy band gap: 2.89 eV (0.12 W/g), 2.39 eV (0.37 W/g), 2.26 eV (0.56 W/g); Surface area: 13.10 m^3/g (0.12 W/g), 13.57 m^3/g (0.37 W/g), 14.35 m^3/g (0.56 W/g)		
Microwave-assisted with extra heating	***Synthesis of Polystyrene (PS) template***: C_8H_8, PVP (2:1 w/w), C_2H_5OH, $Na_2S_2O_8$ ***Hollow ZnO NPs synthesis:*** PS, $Zn(Ac)_2·2H_2O$, NH_4OH ***Glutathione-hollow ZnO NPs synthesis***: Glu, h-ZnO (1:1), CH_3OH	Reaction temp: 70 ºC for 4 h; Drying temp: 27 ºC; Microwave irradiation: 120 ºC for 10 min; Calcination temp: 527 ºC; Sonicate and stir mixture for 1 h	Hollow with cavities; Particle size (TEM): 35 nm; 1483.50 nm (hydrodynamic diameter by DLS); Cavity diameter: 34 nm; Surface area: 17.1 m^2/g (h-ZnO), 12.3 m^2/g (Glu-h-ZnO)	Adsorbent	[103]
Microwave-assisted with extra heating	***Seed layer preparation***: Glass substrate, $Zn(Ac)_2·2H_2O$ deposit by spraying ***Precursor growth***: Seeded substrate, $Zn(NO_3)_2·6H_2O$, HMTA	Deposit spraying temp: 350 ºC; Microwave power: 90 ºC, 180 W for 45 min (4x); Drying temp: 90 ºC Calcination temp: 100 and 350 ºC for 1 h	Rod-like; Particle size: ~ 4.3 µm (ave. length) 100 nm (ave. diameter); Energy band gap: 3.2 eV (100 ºC), 2.9 eV (350 ºC)	Photocatalyst in the degradation of phenol	[104]
Microwave-assisted with extra heating	***Seed layer preparation***: Glass substrate, $Zn(Ac)_2·2H_2O$, C_2H_7NO, $C_3H_8O_2$ deposit by spin coating ***Precursor growth***: Seeded substrate, $Zn(NO_3)_2·6H_2O$, HMTA	Reaction temp: 60 ºC for 1 h; Drying temp: 300 ºC for 10 min; Calcination temp: 100-500 ºC; Microwave power: 90 ºC, for 60 min	Rod-like; Crystallite size: 9-25 nm (seed layer), 38-56 nm (nanorods); Particle size: 180-350 nm (nanorod length); Energy band gap: 3.22-3.30 eV (seed layer), 3.17-3.98 eV (nanorods)	UV Sensor	[105]
Microwave-assisted with extra heating	***Seed layer preparation***: FTO substrate, $Zn(Ac)_2·2H_2O$, C_2H_5OH deposit by spin coating ***Precursor growth***: FTO substrate, $Zn(NO_3)_2·6H_2O$, HMT	Reaction temp: 100 ºC for 15 min; Annealing temp: 350 ºC for 1 h; Microwave power: 1100 W for 20 s (microwave-assisted hydrolysis); Oven temp: 90 ºC for 45 min (hydrothermal process); Drying samples with N_2 gas.	Rod-like; Particle size: 80 nm (diameter of the microwave-assisted sample), 30 nm (diameter of the hydrothermal sample)	CO gas detector	[106]

Method of synthesis	Precursor/Reactant	Synthesis condition	Properties	Applications	Reference
Microwave-assisted without extra heating	$Zn(NO_3)_2{\cdot}6H_2O$, TEA (1:30 v/v)	Microwave power: 640 W for 10 min; Vacuum drying	Crystallite size: ~27 nm	Photocatalyst in the degradation of CTAB	[107]
Microwave-assisted with extra heating	$Zn(Ac)_2{\cdot}2H_2O$, NH_4OH, $ZnCl_2$, $Zn(NO_3)_2{\cdot}6H_2O$, $ZnSO_4.7H_2O$	Microwave power: 2450 MHz, 640 W for 10 min; Vacuum drying: 90 ºC for 12 h; Calcination temp: 600 ºC for 2 h; pH = 9	Flake-like (zinc acetate), Rod-like (zinc nitrate), Spherical (zinc sulfate), Hexagonal tubular (zinc chloride)	Gas sensor for Volatile Organic Compounds (VOC)	[108]
Microwave-assisted with extra heating	$Zn(NO_3)_2{\cdot}6H_2O$, HMT, NaOH	Microwave power: 110, 310, & 710 W, 90, 150 & 220 ºC for 15 min; Calcination temp: 200 ºC for 2 h; pH = 13	Plate-like; Crystallite size: 22.40-24.83 nm; Energy band gap: 3.28-3.38; Surface area: 10.44-18.09 m^2/g; Particle size: 400-600 nm (diameter)		[109]
Microwave-assisted without extra heating	$Zn(NO_3)_2{\cdot}6H_2O$, PEG 400, $NaOH/NH_4OH$	Microwave power: 800 W, 100 ºC for 5 min; Drying temp: 110 ºC for 12 h	Quasi-spherical shape (NaOH with & without PEG), flower-like (NH_4OH with & without PEG); Crystallite size: 29.5 nm (NaOH without PEG), 25.8 nm (NH_4OH without PEG), 34.9 nm (NaOH with PEG), 29.4 nm (NH_4OH with PEG); Particle size: 5 µm (NaOH with & without PEG), > 5 µm (NH_4OH with & without PEG); Surface area: 14.88 m^2/g (NaOH without PEG), 2.75 m^2/g (NH_4OH without PEG), 7.64 m^2/g (NaOH with PEG), 2.03 m^2/g (NH_4OH with PEG)	Catalyst for biodiesel synthesis	[110]
Microwave-assisted without extra heating	***Precursor growth process***: GaN substrate, $Zn(Ac)_2{\cdot}2H_2O$, NaOH	Microwave power: 50 ºC for 2 min; Drying temp: < 100 ºC	Rod-like; Particle size (height & width): 2.2 µm/ 2.5 µm (pH = 6.75), 1.5 µm/0.7 µm (pH = 7.25), 1.5 µm/0.5 µm (pH = 7.75)		[111]
Microwave-assisted with extra heating	$Zn(Ac)_2{\cdot}2H_2O$, KOH	Microwave power: 1000 W for 0, 0.5, 1, 1.5 & 2 min; Drying temp: 80 °C; Calcination temp: 400 °C for 1 h	Rod-like (0 min), Tetrapod (0.5 min), Flower-like (1-2 min); Crystallite size: 53, 59.3, 69.2, 74.5 and 82.4 nm (0-2 min); Particle size (length): 255 nm (0.5 min), 397 nm (1-2 min); Energy band gap: 3.24 eV, 3.23 eV, 3.21 eV, 3.19 eV and 3.17 eV (0-2 min)	Photocatalyst for the degradation of rhodamine B (RhB)	[112]
Microwave-assisted without extra heating	***Seed layer preparation***: p-Si (100) substrate, $Zn(NO_3)_2{\cdot}6H_2O$, $C_6H_{12}N_4$ deposit by RF sputtering ***Precursor growth***:	Annealing temp: 400 ºC for 1 h; Microwave power: 90 ºC for 2 h; Sampled dried with N_2 gas.	Rod-like; Crystallite size: 52.08 nm; Particle size (length): 1 µm	UV detector	[113]

Method of synthesis	Precursor/Reactant	Synthesis condition	Properties	Applications	Reference
	FTO substrate, $Zn(NO_3)_2{\cdot}6H_2O$, HMT				
Microwave-assisted with extra heating	$Zn(NO_3)_2{\cdot}6H_2O$, $C_6H_{12}N_4$ (mole ratio of 3:20, 5:20, 12:20, 20:20 and 30:20)	Microwave power: 750 W, ~120 °C for10 min; Drying temp: 80 °C for 24 h; Calcination temp: 400 °C for 1 h	Spherical to hexagonal rod-like structures; Crystallite size: 16.7-57.9 nm; Particle size: 25 nm to micro/sub micro sizes	Antimicrobial agent	[114]
Microwave-assisted without extra heating	$Zn(Ac)_2{\cdot}2H_2O$, NH_4OH (0.25, 0.5, 1.0, 1.5, 2.0 or 3.0 ml)	Microwave power: 150 °C for 30 min; Drying temp: 150 °C for 2 h pH = 7-11	Hexagonal prism (pH = 7), flower-like (pH = 11); Particle size (width & length): 1 & 5 µm (pH = 7), 100 nm (pH = 8-10)	Photoelectrochemical agent	[115]
Microwave-assisted without extra heating	$Zn(Ac)_2{\cdot}2H_2O$, NaOH	Reaction temp: 60 °C for 2 h; Microwave power: 90 °C for 20 min	Spherical; Particle size : 29 nm		[116]

Table 2. Characteristics of ZnO nanostructures synthesized via different solvothermal routes.

Method of synthesis	Precursor/Reactant	Synthesis condition	Properties	Applications	Reference
Solvothermal with heat treatment	$Zn(Ac)_2{\cdot}H_2O$, ethanol/1-propanol/1-butanol/1-pentanol/1-octanol	Autoclave temp: 170 °C for 4 h	Spherical (1-butanol), rod-like (ethanol, 1-propanol, 1-pentanol, 1-octanol); Particle size: ~12 nm (1-butanol); Crystallite size: 28 nm (ethanol), 14 nm (1-propanol), 12 nm (1-butanol), 13 nm (1-pentanol), 18 nm (1-octanol)		[117]
Microwave-assisted with extra heat treatment	$Zn(NO_3)_2{\cdot}6H_2O$, PVA, Ascorbic acid	Microwave power: 2.45 GHz, 400 W for 3 min; Drying temp: 105 °C for 3 h; Calcination temp: 500 °C for 4 h	Spherical; Band gap: 3.35 eV; Crystallite size: 20-22 nm; Particle size: 70-90 nm (A), 230-280 nm (B), 580-630 nm (C); Surface area: 8.46-10.70 m^2/g	Photocatalyst against Rhodamine-B Antibacterial agent	[118]
Solvothermal synthesis with conventional heating	Zinc salt, dimethyl sulfone, KOH	Reaction temp: 60 °C for 3 & 12 h; Drying temp: 65 °C for 12 h	Spherical; Crystallite size: 4 nm and 10 nm; Particle size (TEM): 4 nm and 10 nm	Antibacterial agent	[119]
Solvothermal synthesis with conventional heating	$Zn(Ac)_2{\cdot}2H_2O$, ethylene glycol, PVP (0.001-0.004 mol)	Refluxing temp: 195 °C for 3 h; Drying temp: 80 °C for 2 h; Calcination temp: 350 °C for 2 h	Spherical to wire-like; Crystallite size: 14.6, 12.8, 47.0 and 81.0 nm; Particle size: 14.8, 12.5, 47.0 & 81.0 nm; Particle length & diameter: 20 µm & 22 nm; Surface area: 91, 121, 71 & 53 m^2/g	Photoanodes	[120]
Solvothermal synthesis with	$Zn(Ac)_2{\cdot}2H_2O$, DMAc:H_2O (1:0, 4:1, 3:2, 2:3, 1:4)	Reaction temp: 95 °C for 3 h; Drying temp: 80 °C for overnight; pH = 6.12-6.86	Quasi-spherical, dumbbell shape, rod-like; Ave. diameter: 90 nm-0.7 µm; Energy band gap: 3.27-3.42 eV		[121]

Method of synthesis	Precursor/Reactant	Synthesis condition	Properties	Applications	Reference
conventional heating					
Solvothermal synthesis with conventional heating	$Zn(Ac)_2{\cdot}2H_2O$, ethanol, NaOH, SDS/PVP/PEG-10000	Reaction temp: 110 °C for 10 h	Spherical (surfactant free), Hexagonal disc (SDS presence), Hexagonal bilayer disk (PVP), Flower-like (PEG-10000); Particle size: 80-150 nm (surfactant free), 300 & 200 nm for length & thickness (SDS), 6 µm and 4 µm for length & thickness (PVP), ~200 nm as average diameter (PEG-10000); Band gap: 3.24 eV (surfactant free), 3.20 eV (SDS), 3.15 eV (PVP), and 3.24 eV (PEG-10000)	Photocatalyst in the degradation of Rhodamine-B (Rh-B).	[122]
Microwave-assisted without heat treatment	$Zn(Ac)_2{\cdot}2H_2O$, ethylene glycol, H_2O (1.5 wt. %)	Reaction temp: 70 ºC; Microwave radiation: 1, 2, & 3 kW, 2.45 GHz, 12 min, 4 bar; Drying: freeze drying	Spherical shape, hexagonal shape; Particle size: 25-50 nm; Crystallite size: 23-48 nm; Surface area: 40.1-40.6 m^2/g		[123]
Solvothermal synthesis with conventional heating	$Zn(Ac)_2{\cdot}2H_2O$, ethanol, KOH	Reaction temp: 60 °C for 3 h; Drying temp: room temp.	Spherical; Crystallite size: 10.08 nm; Particle size (TEM/BET): 7.4/9.7 nm; Surface area: 101.32 m^2/g		[124]
Solvothermal synthesis with conventional heating	$Zn(Ac)_2{\cdot}2H_2O$, ethanol, NaOH, CTAB, wood samples, FAS-17	Reaction temp: 2 h at room temperature; Autoclave temp: 90 °C for 4 h; Drying temp: 45 °C for 24 h.	Rod-like; Particle size: 85 nm & 1.5 µm (diameter & length)	UV resistor	[125]
Microwave-assisted without heat treatment	$Zn(NO_3)_2{\cdot}6H_2O$, urea (1:5 molar ratio),	Microwave irradiation: 150 °C for 15 min; Drying temp: 50 ºC overnight	Flower-like; Particle size (breadth): 10 nm to micron		[126]
Microwave-assisted without heat treatment	$Zn(Ac)_2.2H_2O$ (1, 2, 4 & 8 mM), diethylene glycol, oleic acid	Microwave power: 250 °C for 15 min; Drying temp: 80 °C	Spherical; Particle size: 4-14 nm		[127]
Microwave-assisted with heat treatment	$Zn(Ac)_2.2H_2O$, Isopropanol, Diethanolamine	Microwave power: 150, 175 & 200 °C; Calcination temp: 100 °C for 2 h	Energy band gap: 3.38-3.94 eV	Photodetector	[128]
Microwave-assisted with heat treatment	$Zn(Ac)_2.2H_2O$, NaOH, Dimethylformamide	Microwave power: 300 W, 1 h; Drying temp: 60 °C for 4 h; Calcination temp: 500 °C	Spherical; Crystallite size: 24 nm and 26 nm (calcined sample); Energy band gap: 3.26 eV and 3.20 eV (calcined sample)	Dye (methyl orange) removal agent	[129]

Method of synthesis	Precursor/Reactant	Synthesis condition	Properties	Applications	Reference
Microwave-assisted without heat treatment	$Zn(Ac)_2.2H_2O$, NaOH, Triton X-100, H_2O / 2-ethoxyethanol (ET) / ethylene glycol (EG).	Microwave power: 300 W for 3 min; Drying temp: room temp for 72 h	Rod-like (H_2O & ET), Flower-like (EG); Crystallite size: 52.64 nm (H_2O), 63.70 nm (ET), 24.02 nm (EG); Energy band gap: 3.35 eV (ET), 3.38 eV (H_2O), 3.42 eV (EG)	Photocatalyst in the degradation of methylene blue	[130]
Microwave-assisted without heat treatment	$ZnCl_2$, $C_{18}H_{33}NaO_2$, $C_{16}H_{37}NO$, CH_3OH, $C_{36}H_{66}O_4Zn$, C_4H_8O	Microwave irradiation: 125, 150, 175 & 200 °C for 5 min	Spherical; Particle size (radius/width): 2.6/0.2 nm (125 °C), 2.7/0.3 nm (150 °C), 3.1/0.3 nm (175 °C), 3.8/0.5 nm (200 °C); Energy band gap:): 3.44 eV (125 °C), 3.40 eV (150 °C), 3.38 eV (175 °C), 3.36 eV (200 °C); Crystallite size:): 4.55 nm (125 °C), 5.88 nm (150 °C), 6.84 nm (175 °C), 8.00 nm (200 °C)		[131]
Microwave-assisted with and without heat treatment	$Zn(Ac)_2.2H_2O$, diethylene glycol, oleic acid, Toulene, Si substrate	Microwave power: 220 & 250 °C for 10 & 15 min; Drying temp: 80 °C for 30min; Drying temp of substrate: 100 °C for 3 h; Calcination temp of substrate: 400 °C for 3 h	Particle size : 5-12 nm	Optoelectronic devices	[132]

Table 3. Characteristics of ZnO nanostructures synthesized via different sol-gel routes.

Method of synthesis	Precursor/Reactant	Synthesis condition	Properties	Applications	Reference
Sol-gel without heat treatment	$Zn(Ac)_2.2H_2O$, CH_3OH, NaOH	Sonication power: 750 W for 30 min; Drying temp: 80 °C; pH = 5-12	Particle size: 1.3 nm (pH, 7) and 73.8 nm (pH, 12) Crystallite size: 10.94 (pH, 7), 17.44 (pH, 8), 38.27 (pH, 10), 74.04 (pH, 12)		[133]
Sol-gel without heat treatment	$ZnCl_2$, NaOH	Reaction temp: 50-90 °C; Dripping time: 20-60 min; Drying temp: 70 °C	Crystallite size: 21-37 nm	Photocatalyst in the degradation of dyes	[134]
Sol-gel with heat treatment	$ZnSO_4 \cdot 7H_2O$, NaOH (1:1, 1:2, & 1:3 mole ratio)	Reaction time: 8, 10 & 12 h; Drying temp: 100 °C; Calcination temp: 300, 500, & 700 °C for 2 h	Nanoplatelets (1:1, 10 h, 300 °C), nanospheres (1:2, 8 h, 700 °C), nanoplatelets and nanorod (1:3, 12 h, 500 °C); Particle size: 164-197 nm (300 °C), 1.73-167 nm (500 °C), 85-157 nm (700 °C); Crystallite size: 40.57 nm	Reinforcement agent for polymers	[135]
Sol-gel with heat treatment	$Zn(NO_3)_2 \cdot 6H_2O$, PVA	Reaction temp: 80 °C for 60 h; Drying temp: 100 °C for 24 h; Calcination temp: 400-700 °C	Spherical; Crystallite size: 15-51 nm (400-550 °C); Particle size (TEM): 15 nm (400 °C), 25 nm (500 °C)	Photocatalyst in the degradation of phenol	[136]

Table 4. Characteristics of doped-ZnO nanostructures synthesized via different techniques.

Method of synthesis	Composite	Precursor/Reactant	Synthesis condition	Properties	Applications	Reference
Solvothermal	Ag-ZnO & Pt-ZnO	$Zn(NO_3)_2{\cdot}6H_2O$, $AgNO_3$, $Pt(C_5H_7O_2)_2$, CTAB	Reaction temp: room temp for 1 h; Autoclave temp: 120 °C 3 & 6 h; Drying temp: 80 °C	Nanowires; Crystallite size: 23-15.9 nm (ZnO), 193.6-63.6 nm (Pt-ZnO), 12.9-11.5 nm (Ag-ZnO); Particle size (TEM): 67-138 nm (ZnO), 133-143 nm (Ag-ZnO), 101-194 nm (Pt-ZnO) Surface area: 5-33 m^2/g (ZnO), 23-43 m^2/g (Ag-ZnO), 4-15 m^2/g (Pt-ZnO); Energy band gap: 3.21-3.24 eV (ZnO), 3.23-3.29 eV (Ag-ZnO), 3.23-3.24 eV (Pt-ZnO)	Photocatalyst in the degradation of dyes	[137]
Hydrothermal	Ce-ZnO	ZnO, CeO_2, NaOH/KOH, n-butyl amine	Autoclave temp: 100 °C for 12 h	Hexagonal	Photocatalyst in the degradation of synthetic wastewater	[138]
Hydrothermal	ZnO-CdS-Ag	$Zn(NO_3)_2{\cdot}6H_2O$, $C_2H_4O_3$, KOH, $Cd(NO_3)_2{\cdot}4H_2O$, C_2H_5NS, $AgNO_3$, N_2H_4	Reaction temp (ZnO): 60 °C for 2 h; Autoclave temp (ZnO): 120 °C for 48 h; Drying temp (ZnO): 120 °C for 8 h; Reaction time (ZnO-CdS): 1 h; Drying temp (ZnO-CdS): 70 °C; Reaction time (ZnO-CdS-Ag): 1 h; Drying temp: 70 °C	Rod-like; Crystallite size: 23 & 15 nm (ZnO & CdS); Surface area: 18.9 m^2/g (ZnO-CdS-Ag)	Photocatalyst against *E. coli*	[139]
Hydrothermal	ZnO-CdS (25:75, 50:50 and 75:25)	$Zn(NO_3)_2{\cdot}6H_2O$, $ZnCl_2$, Thiourea	Reaction time (ZnO): 1 h; pH = 12; Autoclave temp (ZnO): 150 °C for 3 h; Autoclave temp (CdS): 160 °C for 12 h; Drying temp (CdS): 100 °C; Calcination temp (ZnO-CdS): 500 °C for 3 h	Flake-like (ZnO-CdS), Hexagonal (ZnO), cubic (CdS); Crystallite size: 13-33 nm (25:75), 17-35 nm (50:50), 21-38 nm (75:25); Energy band gap: 3.71 eV (25:75), 3.49 eV (50:50), 3.35 eV (75:25)		[140]
Microwave-assisted hydrothermal	ZnO-Graphene oxide (GO)	$Zn(NO_3)_2{\cdot}6H_2O$, PVP, HMTA	Microwave power (ZnO/ZnO-GO): 300 W, 100 °C for 1 h/45 min; Drying temp (ZnO/ZnO-GO): 85 °C	Star-like (ZnO), flake-like sheets (GO); Particle size: 550 nm (ZnO); Surface area: 34.3 m^2/g (ZnO-GO)	Electrocatalyst	[141]

Method of synthesis	Composite	Precursor/Reactant	Synthesis condition	Properties	Applications	Reference
Microwave-assisted hydrothermal	Ag–ZnO	Carbinol, $Zn(Ac)_2.2H_2O$, $AgNO_3$, CTAB, $NaBH_4$	Microwave power (ZnO): 900 W, 5, 10 & 15 min; Microwave power (Ag-ZnO): 900 W, 20 min	Spherical (ZnO-5 min), hexagonal (ZnO-10 min), spike-like (ZnO-15 min), spike-like (Ag-ZnO-20 min); Particle size: 400-450 nm (ZnO); Length & thickness of Ag-ZnO was 1 µ & 30-40 nm; Energy band gap: 3.72 eV (Ag-ZnO)	Sensor to biomolecules	[142]
Microwave-assisted hydrothermal		CTAB, $Zn(Ac)_2.2H_2O$, $AgNO_3$, Na_2O_2 mole ratio; CTBA:Zn:Ag = 1:1.5:0.05)	Reaction time: 30 min, Autoclave temp: 200 °C, Microwave irradiation: 300 W, 200 °C for 3, 4.5 & 6 h, Drying temp: 80 °C, Calcination temp: 300 °C for 2 h	Rod-like stacked into a chrysanthemum-like (flower) structure; Crystallite size: 4.1, 3.3, 3.2 & 3.4 nm (ZnO, Ag-ZnO-3, 4.5 & 6 h); Energy band gap: 3.21, 3.17, 3.14, 3.12 eV (ZnO, Ag-ZnO-3, 4.5 & 6 h); Surface area: 1.05, 6.71, 6.40, 6.74 m^2/g (ZnO, Ag-ZnO-3, 4.5 & 6 h)	Photocatalyst in the degradation of RhB	[143]
Sol-gel	Al-ZnO	$Zn(Ac)_2.2H_2O$, $Al(NO_3)_3$ (0, 3, 6, 9 & 12% %wt)	Reaction temp: 80 °C for 1 h; Drying temp: 100 °C; Calcination temp: 600 °C for 4 h	Rod-like (ZnO), spherical (Al-ZnO); Crystallite size: 78.8, 49.6, 29.9, 35.0 & 52.4 nm (Al-ZnO-0, 3, 6, 9 & 12%)	Sensor to NH_3 gas	[144]
Microwave-assisted hydrothermal	ZnO-N	$Zn(Ac)_2.2H_2O$, NaOH, urea (5%)	Reaction time (ZnO/ZnO-N): 10 min; Microwave power (ZnO/ZnO-N): 800 W, 100 °C for 1 h	Flower-like with array of nanorods Particle size (Length): 1.2 - 1.7 µm (ZnO), 2.0 - 2.4 µm (ZnO-N)	Photocatalyst in the degradation of Rh-B & Cr (VI)	[145]
Microwave solvothermal	Co-Mn-ZnO	$Zn(Ac)_2.2H_2O$, $Mn(Ac)_2.4H_2O$, $Con(Ac)_2.4H_2O$,	Reaction temp: 70 °C; Microwave power: 100%, 190 °C, 25 min; Drying temp: freeze drying	Spherical; Particle size: 20–40 nm; Surface area: 45.8-56.4 m^2/g (Co-Mn-ZnO), 39.8 m^2/g (ZnO); Crystallite size: 19-22 nm (Co-Mn-ZnO), 22 nm (ZnO)		[146]
Sol-gel	Zr-Cr/ZnO	$Zn(NO_3)_2{\cdot}6H_2O$, $Cr(NO_3)_3{\cdot}9H_2O$, oxalic acid	Aging conditions: 2 h at room temperature, 75 °C for 2 h and 120 °C for another 10 h in an oven; Calcination temp: 400 °C for 6 h	Hexagonal nanoplates and nano-polyhedron shapes	Catalyst	[147]

Method of synthesis	Composite	Precursor/Reactant	Synthesis condition	Properties	Applications	Reference
Microwave-assisted hydrothermal	Mn-ZnO	$Mn(Ac)_2 \cdot 4H_2O$ (1, 5, & 10 wt%), $Zn(Ac)_2.2H_2O$	Reaction temp: 30 °C; Microwave power: 300W, 95 °C for 10, 20 & 30 min; Drying temp: 60 °C for 24 h; Calcination temp: 500 °C for 2 h.	Rod-like; Particle size (diameter): 600-50 nm	Sensors	[148]
Microwave solvothermal synthesis		$Zn(Ac)_2.2H_2O$, $Mn(Ac)_2 \cdot 4H2O$ (1, 5, 10, 15, 20, 25 mol % Mn)	Reaction temp: 70 °C; Microwave power: 600 W, 2.45 GHz, 200 °C for 25 min; Drying mode: freeze drying	Spherical shape, flower-like (5-25 mol %); Particle size: 30–35 nm to 15–25 nm (0-20 mol %.), 20–25 nm (25 mol %); Crystallite size: 22, 21, 18, 17, 18, 16, & 19 nm (0, 1, 5, 10, 15, 20 & 25 mol %); Specific area: 28, 30, 24, 20, 21, 17 & 19 m^2/g (0, 1, 5, 10, 15, 20 & 25 mol %)		[149]
Microwave assisted method	Co-ZnO	$Zn(Ac)_2.2H_2O$, $C_4H_6CoO_4$, Urea, Ethylene glycol	Reaction time: 1 h; Microwave temp: 80 °C; Calcination temp: 300 °C for 1 h	Crystallite size 18 – 28 nm Energy band gap: 2.24-3.26 eV Spherical		[150]
Microwave assisted method		$Zn(Ac)_2.2H_2O$, diethylene glycol (DEG), $Co(II)(Acac)_2$, oleic acid	Microwave power: 250 °C for 25 min; Calcination temp: 400 °C; Drying temp: 80 °C	Hexagonal; Crystallite size: 8.9-9.9 nm, 16–19 nm (calcined sample); Particle size: 15–35 nm; Energy band gap: 2.79-3.23 eV	Electroluminescent material for polymer light emitting diodes	[132]
Microwave-Assisted Synthesis	AL-ZnO, Ga-ZnO, Al-Ga-ZnO	$Zn(Ac)_2.2H_2O$, $AlCl_3 \cdot 6H_2O$, $Ga(NO_3)_3 \cdot xH_2O$, diethylene glycol (DEG)	Reaction time: 1 h; Microwave power: 2.45 GHz, 1500 W, 200 °C for 30 min; Drying temp: 60 °C for 1 h; Calcination temp: 450 °C for 1 h	Spherical; Particle size: 100 nm (Ga-ZnO), 250 nm (Al-ZnO), ~85 nm (Al-Ga-ZnO)	Conducting material for Transparent conducting oxides (TCO) coatings	[151]
Reflux method	Cu-ZnO	$Zn(NO_3)_2 \cdot 6H_2O$, $CuCl_2.2H_2O$	Reflux time (ZnO): 3 h; Reflux time (Cu-ZnO): 3-9 h; Drying temp (Cu-ZnO): 80 °C.	Cube-like, maize corn seed-like, rod-like (ZnO), maize corn seed-like (Cu-ZnO); Crystallite size: 28 nm (ZnO), 20 nm (Cu-ZnO); Particle	Photocatalyst in the degradation of methyl orange (MO)	[152]

Method of synthesis	Composite	Precursor/Reactant	Synthesis condition	Properties	Applications	Reference
				size (diameter & length): 30–35 nm & 90 nm (Cu-ZnO); Energy band gap: 3.38-3.46 eV (Cu-ZnO)		
Solvent-thermal technique	Fe_3O_4/ZnO	$C_6H_5Na_3O_7 \cdot 2H_2O$, CH_3-COONa, $FeCl_3 \cdot 6H_2O$, diethylene glycol (DEG), ethylene glycol (EG), tetraethyl orthosilicate (TEOS)	Reaction temp (ZnO): 40 °C for 3 h; Drying temp (ZnO & composite): 70 °C for 3 h; Microwave temp (composite): 160 °C for 15, 30, 60 min,	Spherical; Surface area: 22.30 m^2/g (composite with 10% Fe_3O_4), 27.52 m^2/g (composite with 20% Fe_3O_4), 20.10 m^2/g (composite with 30% Fe_3O_4); Energy band gap: 3.21-3.24 eV	Photocatalyst in the degradation of 4-Nitrophenol (4-NP)	[153]
Solvothermal	CeO_2-ZnO	$Zn(Ac)_2.2H_2O$, $CeCl_3 \cdot 7H_2O$, $Na_3C_6H_5O_7$,	Autoclave temp: 200 °C for 10 h; Calcination temp: 500 °C for 2 h	Chain-like structure; Crystallite size: 9.5 nm; Surface area: 40.9 m^2/g,	Gas sensor and in diagnosis of diabetes and chemical detection	[154]
Microwave method	Fe-ZnO	$Zn(OAc)_2.2H_2O$, NaOH, $Fe(NO_3)_3 \cdot 9H_2O$	Microwave power: 140 W for 2 min (ZnO); Drying temp: 200 °C for 1 h (ZnO); Drying temp: 120 °C for 4–5 min (Fe-ZnO); Calcination temp: 300 °C	Energy band gap: 3.20-3.24 eV; Particle size (diameter): 17.4-11.29 nm (Fe-ZnO)	Anti-reflector coating	[155]
Microwave-assisted hydrothermal		$Zn(NO_3)_2 \cdot 6H_2O$, $Fe(NO_3)_3 \cdot 9H_2O$ (0, 1, 3, 5, 7 & 10% mole),	Microwave power: 700 W, 5.8–6.2 MPa, 20 min; Drying temp: 60◦C by 18 h; pH = 9.5	Rod-like, hexagonal prism; Crystallite size: 130 nm (5% Fe), 60 nm (7% Fe), 30 nm (10% Fe), 60 nm (< 5% Fe); Particle size: 392-296 nm (0-10% Fe)	Useful in biomedical applications	[156]
Hydrothermal method	Zn-Al-Gd	$Zn(Ac)_2.2H_2O$, $Al(NO_3)_3 \cdot 2H_2O$, $Gd(NO)_3 \cdot 6H_2O$, NH_4OH	Reaction time: 3 h; Autoclave temp: 160 °C for 24 h; calcination temp: 600 °C; pH = ~9	Mixture of urchin-like and rod-like structures; Crystallite size: 67-47 nm		[157]
Hydrothermal method	Eu-ZnO	$Zn(Ac)_2.2H_2O$, $Eu(CH_3CO_2)_3 \cdot xH2O$ (1, 3 & 5 wt%)	Reaction time: 20 min; Autoclave temp: 150 °C for 8 h; Drying temp: 80 °C for 24 h, pH = 10	Spherical (undoped & doped); Crystallite size: 26 nm (undoped), 24, 15, & 18 nm (1%, 3% & 5% Eu); Energy band gap: 3.18 eV (undoped), 3.05, 3.00, & 2.94 eV (1%, 3% & 5% Eu)	Optoelectronic devices	[158]
Single-step aerosol process	ZnO-Carbon dots	$Zn(NO_3)_2 \cdot 6H_2O$, $C_6H_8O_7$,	Reaction time: 1 h; Heating temp: 500, 550, 600 & 650 °C; Annealing temp: 600 °C for 3 h	Spherical	Photocatalyst for CO_2 reduction	[159]

Method of synthesis	Composite	Precursor/Reactant	Synthesis condition	Properties	Applications	Reference
Microwave-assisted	Al_2O_3-ZnO	Commercial ZnO NPs, Aluminium triisopropoxide (0.5, 1.0 & 1.5 g)	Grinding time: 10 min; Microwave temp: 500 W, 2.45 GHz, 70 ^oC for 5 min; Aging time: 3 h; Drying temp: 110 ^oC for 2 h	Particle size: 20-30 nm (ZnO),	Photocatalyst in the degradation of methylene blue (MB)	[160]

3. Conclusions

The multi-functionality of ZnO nanomaterials continues to grow as the developments of new methods to their synthesis are explored. These new methods allow for the control of the morphology, which subsequently affects their properties in producing innovative devices for its various applications. The improvement of microwave technology has made it easy to synthesize different desirable morphologies of nanomaterials with speed and purity. This technology is applied to different synthesis methods (solvothermal, hydrothermal, and sol-gel), it was possible to obtain desirable morphologies as the reaction mechanism could be controlled. Besides the heating mechanism, other factors such as the type of precursor, surfactants, alkaline source, annealing temperature, and dopants affect the morphological structure.

Funding

This research was funded by Universiti Malaysia Sarawak, Tun Openg Chair, with research grant code: F07/TOC/1738/2018.

Acknowledgments

The authors would like to thank the funding provided by Universiti Malaysia Sarawak, Tun Openg Chair, with research grant code: F07/TOC/1738/2018. We also acknowledge the contribution of colleagues from the Faculty of Resource Science and Technology (FRST), Geochemistry Laboratory, and Analytical Laboratory, Universiti Malaysia Sarawak.

Conflict of Interest

The authors declare no conflict of interest.

References

1. Jiang, J.; Pi, J.; Cai, J. The advancing of zinc oxide nanoparticles for biomedical applications. *Bioinor. Chem. Appls* **2018**, 1-18, https://doi.org/10.1155/2018/1062562.
2. Chaudhary, S.; Umar, A.; Bhasin, K.K.; Baskoutas, S. Chemical sensing applications of ZnO nanomaterials. *Mater.* **2018,** *11*, 1-38, https://doi.org/10.3390/ma11020287.
3. Sarmah, K.; Pratihar, S. Synthesis, characterization and photocatalytic application of iron oxalate capped Fe, Fe-Cu, FeCo, and Fe-Mn oxide nanomaterial. *ACS Sustain. Chem. Eng.* **2017,** 5, 310-324, https://doi.org/10.1021/acssuschemeng.6b01673.
4. Das, P.; Sarmah, K.; Hussain, N.; Pratihar, S.; Das, S.; Bhattacharyya, P.; Patil, S.A.; Kim, H.S.; Iqbal, M.; Khazie, A.; Bhattacharyya, S.S. Novel synthesis of an iron oxalate capped iron oxide nanomaterial; a unique soil conditioner and slow release eco-friendly source of iron sustenance in plants. *RSC Adv.* **2016**, *6*, 103012-25, https://doi.org/10.1039/C6RA18840K.
5. Alshamsi, H.A.H.; Hussein, B.S. Hydrothermal preparation of silver doping zinc oxide nanoparticles: synthesis, characterization and photocatalytic activities. *Orient. J. Chem*. **2018**, *34*, 1898-1907, https://dx.doi.org/10.13005/ojc/3404025.
6. Jin, S-E.; Jin, H-E. Synthesis, characterization, and three-dimensional structure generation of zinc oxide-based nanomedicine for biomedical applications. *Pharma.* **2019**, *11*, 575, 1-26, https://doi.org/10.3390/pharmaceutics11110575.
7. Kwoka, M.; Lyson-Sypien, B.; Kulis, A.; Maslyk, M.; Borysiewicz, M.A.; Kaminska, E.; Szuber, J. Surface properties of nanostructured, porous ZnO thin films prepared by direct current reactive magnetron sputtering. *Mater.* **2018**, *11*, 131, https://doi.org/10.3390ma11010131.

8. Ren, X.; Zi, W.;Wei, Q.; Liu, S. Fabrication gallium/graphene core–shell Nanoparticles by pulsed laser deposition and their applications in surface enhanced Raman scattering. *Mater. Lett*. **2015**, *143*, 194–196, https://doi.org/10.1016/j.matlet.2014.12.089.
9. Chhikara, D.; Senthil, K.M.; Srivatsa, K.M.K. On the synthesis of Zn/ZnO core–shell solid microspheres on quartz substrate by thermal evaporation technique. *Superlatt. Microstruc.* **2015**, *82*, 368–377, https://doi.org/10.1016/j.spmi.2015.02.036.
10. Varnamkhasti, M.G.; Fallah, H.R.; Zadsar, M. Effect of heat treatment on characteristics of nanocrystalline ZnO films by electron beam evaporation. *Vacuum* **2012,** *86*, 871–875, https://doi.org/10.1016/j.vacuum.2011.03.017.
11. Maleki-Ghaleh, H.; Shahzadeh, M.; Hoseinizadeh, S.A.; Arabi, A.; Aghaie, E.; Siadati, M.H. Evaluation of the photoelectro-catalytic behavior of nano-structured ZnO films fabricated by electrodeposition process. *Mater. Lett.* **2016**, *169*, 140–143, https://doi.org/10.1016/j.matlet.2016.01.090.
12. Zhu, L.; Li, Y.; Zeng, W. Hydrothermal synthesis of hierarchical flower-like ZnO nanostructure and its enhanced ethanol gas-sensing properties. *Appl. Surf. Sci* **2018**, *427*, 281-287, https://doi.org/10.1016/j.apsusc.2017.08.229.
13. Brahma, S.; Shivashankar, S.A. Microwave irradiation assisted rapid growth of ZnO nanorods over metal coated/electrically conducting substrate. *Mater. Lett* **2020**, *264*, 127370, https://doi.org/10.1016/j.matlet.2020.127370.
14. Dwivedi, S.; Wahab, R.; Khan, F.; Mishra, Y.K.; Musarrat, J.; Al-Khedhairy, A.A. Reactive oxygen species mediated bacterial biofilm inhibition via zinc oxide nanoparticles and their statistical determination. *PLOS ONE* **2014**, *9*, e111289, https://doi.org/10.1371/journal.pone.0111289.
15. Sahu, K.; Kuriakose, S.; Singh, J.; Satpati, B.; Mohapatra, S. Facile synthesis of ZnO nanoplates and nanoparticle aggregates for highly efficient photocatalytic degradation of organic dyes. *J. Phys. Chem. Sol.* **2018**, *121*, 186-195, https://doi.org/10.1016/j.jpcs.2018.04.023.
16. Ghorbani, H.R.; Mehr, F.P.; Pazoki, H.; Rahmani, B.M. Synthesis of ZnO nanoparticles by precipitation method. *Orient. J. Chem*. **2015**, *31*, 1219-1221, https://doi.org/10. 13005/ojc/310281.
17. Gopal, V.R.V.; Kamila, S. Effect of temperature on the morphology of ZnO nanoparticles: a comparative study. *Appl. Nanosci.* **2017**, *7*, 75–82, https://doi.org/10.1007/s13204-017-0553-3.
18. Mahdavi, R.; Talesh, S.S.A. The effect of ultrasonic irradiation on the structure, morphology and photocatalytic performance of ZnO nanoparticles by sol-gel method. *Ultrason. Sonochem*. **2017**, *39*, 504-510, https://doi.org/10.1016/j.ultsonch.2017.05.012.
19. Droepenu, E.K.; Wee, B.S.; Chin, S.F.; Kok, K.Ying.; Zaini, B.A.; Asare, E.A. Comparative evaluation of antibacterial efficacy of biological synthesis of ZnO nanoparticles using fresh leaf extract and fresh stem-bark of Carica papaya. Nano Biomed. Eng. 2019, 11, 264-271, https://doi.org/10.5101/nbe.v11i3.p264-271.
20. Ghanbari, M.; Bazarganipour, M.; Salavati-Niasari, M. Photodegradation and removal of organic dyes using cui nanostructures, green synthesis and characterization. *Separa. Purific. Technol.* **2017**, *173*, 27-36, https://doi.org/10.1016/j.seppur.2016.09.003.
21. Kalpana, V.N.; Rajeswari, V.D. A review on green synthesis, biomedical applications, and toxicity studies of ZnO NPs. *Bioinorg. Chem. Appls* **2018**, 1-12, https://doi.org/10.1155/2018/3569758.
22. Chu, H.O.; Wang, Q. Shi, Y-J.; Song, S.; Liu, W.; Zhou, S.; Gibson, D.; Alajlani, Y.; Li. C. Structural, optical properties and optical modelling of hydrothermal chemical growth derived ZnO nanowires. *Trans. Nonferrous Met. Soc. China* **2020**, *30*, 191-199, https://doi.org/10.1016/S1003-6326(19)65191-5.
23. Rocha, L.S.R.; Foschini, C.R.; Silva, C.C.; Longo, E.; Simoes, A.Z. Novel ozone gas sensor based on ZnO nanostructures grown by the microwave-assisted hydrothermal route. *Ceram. Int.* **2016**, *42*, 4539-4545, https://doi.org/10.1016/j.ceramint.2015.11.145.
24. Li, X.; Wang, C.; Zhou, X.; Liu, J.; Sun, P.; Lu, G. Gas sensing properties of flower-like ZnO prepared by microwave-assisted technique. *RSC Adv*. **2014**, *4*, 47319-47324, https://doi.org/10.1039/C4RA07425D.
25. Vahidi, A.; Vaghari, H.; Najian, Y.; Najian, M.J.; Jafarizadeh-Malmiri, H. Evaluation of three different green fabrication methods for the synthesis of crystalline ZnO nanoparticles using Pelargonium zonale leaf extract. *Green Proc. & Synth*. **2019**, *8*, 302-308, https://doi.org/10.1515/gps-2018-0097.
26. Satheshkumar, M.; Anand, B.; Muthuvel, A.; Rajarajan, M.; Mohana, V.; Sundaramanickam, A. Enhanced photocatalytic dye degradation and antibacterial activity of biosynthesized ZnO-NPs using curry leaves extract with coconut water. *Nanotechnol. Environ. Eng*. **2020**, *5*, 1-11, https://doi.org/10. 1007/s41204-020-00093-x.

27. Wojnarowicz, J.; Chudoba, T.; Lojkowski, W. A Review of microwave synthesis of zinc oxide nanomaterials: reactants, process parameters and morphologies. *Nanomater*. **2020**, *10*, 1086, 1-140, https://doi.org/10.3390/nano10061086.
28. Saberon, S.I.; Maguyon-Detras, M.C.; Migo, M.V.P.; Herrera, M.U.; Manalo, R.D. Microwave-assisted synthesis of zinc oxide nanoparticles on paper. Key Engineering *Mater*. **2018**, *775*, 163-168, https://doi.org/10.4028/www.scientific.net/KEM.775.163.
29. Yang, G.; Park, S.-J. Conventional and microwave hydrothermal synthesis and application of functional materials: A review. *Mater.* **2019**, *12*, 1177, https://doi.org/10.3390/ma12071177.
30. Jalouli, B.; Abbasi, A.; Khoei, M.S.M. A comment on: "Conventional and microwave hydrothermal synthesis and application of functional materials: A review". *Mater*. **2019**, *12*, 3631, https://doi.org/10.3390/ma12213631.
31. Rana, K.; Rana, S. Microwave reactors: A brief review on its fundamental aspects and applications. *Open Acc. Lib. J.* **2014**, *1*, 1–20, https://doi.org/10.4236/OALIB.1100686
32. Kim, T.; Lee, J.; Lee, K.-H. Microwave heating of carbon-based solid materials. *Carbon Lett.* **2014**, *15*, 15–24, https://doi.org/10.5714/CL.2014.15.1.015.
33. Mohan, S.; Vellakkat, M.; Aravind, A.; Rekha, U. Hydrothermal synthesis and characterization of zinc oxide nanoparticles of various shapes under different reaction conditions. *Nano Express* **2020**, 1-25, https://doi.org/10.1088/2632-959X/abc813.
34. Ming, O.U.; Lin, M.A.; Limei, X.U.; Haizhen, L.I.; Zhuomei, Y.; Zhifeng, L.A.N. Microwave-assisted synthesis of hierarchical ZnO nanostructures and their photocatalytic properties. MATEC Web of Conferences **2016**, 67, 1-7.
35. Suwanboon, S.; Klubnuan, S.; Jantha, N.; Amornpitoksuk, P.; Bangrak, P. Influence of alkaline solutions on morphology of ZnO prepared by hydrothermal method for using as photocatalyst and bactericidal agent. *Mater. Lett.* **2014**, *115*, 275-278, https://doi.org/10.1016/j.matlet.2013.10.066.
36. Zhu, L.; Li, Y.; Zeng, W. Hydrothermal synthesis of hierarchical flower-like ZnO nanostructure and its enhanced ethanol gas-sensing properties. *Appl. Surf. Sci*. **2018**, *427*, 281-287, https://doi.org/10.1016/j.apsusc.2017.08.229.
37. Zhou, Q.; Xie, B.; Jin, L.; Chen, W.; Li, J. Hydrothermal synthesis and responsive characteristics of hierarchical zinc oxide nanoflowers to sulfur dioxide. *J. Nanotechnol*. **2016**, 1-6, https://doi.org/10.1155/2016/2083948.
38. Perillo, P.M.; Atia, M.N.; Rodríguez, D.F. Studies on the growth control of ZnO nanostructures synthesized by the chemical method. *Revista Matéria* **2018**, *22*, 1-7, https://doi.org/10.1590/S1517-707620180002.0467.
39. Alver, U.; Tanriverdi, A.; Akgul, O. Hydrothermal preparation of ZnO electrodes synthesized from different precursors for electrochemical supercapacitors. Synthetic *Mater*. **2016**, *211*, 30-34, https://doi.org/10.1016j.synthmet.2015.11.008.
40. Amin, G.; Asif, M.H.; Zainelabdin, A.; Zaman, S.; Nur, O.; Willander, M. Influence of pH, precursor concentration, growth time, and temperature on the morphology of ZnO nanostructures grown by the hydrothermal method. *J. Nanomater*. **2011**, 1-10, https://doi.org/10.1155/2011/269692.
41. Sarangi, S. N., Acharya, S., and Biswal, S. K. (**2018**). Different morphology of ZnO nanostructures using hydrothermal and electro-deposition technique. Aspects in Mining and Mineral Science, 1, AMMS.000515, 92-93.
42. Li, J.; Wu, Q.; Wu, J. Synthesis of nanoparticles via solvothermal and hydrothermal methods. *Handb. Nano*. **2016**, 295–328, https://doi.org/10.1007/978-3-319-15338-4_17.
43. Zak, A.K.; Razali, R.; Majid, W.H.A.; Darroudi, M. Synthesis and characterization of a narrow size distribution of zinc oxide nanoparticles. *Int. J. Nanomed*. **2011**, *6*, 1399–1403, https://doi.org/10.2147/IJN.S19693.
44. Bai, X.; Li, L.; Liu, H.; Tan, L.; Liu, T.; Meng, X. Solvothermal synthesis of ZnO nanoparticles and anti-infection application in vivo. *ACS Appl. Mater. Interface* **2015**, *7*, 1308–1317, https://doi.org/10.1021/am507532p.
45. Šarić, A.; Štefanić, G.; Dražić, G.; Gotić, M. Solvothermal synthesis of zinc oxide microspheres. *J. Alloys Compd*. **2015**, 652, 91−99, https://doi.org/10.1016/j.jallcom.2015.08.200.
46. Šarić, A.; Gotić, M.; Štefanić, G.; Dražić, G. Synthesis of ZnO particles using water molecules generated in esterification reaction. *J. Mol. Struct*. **2017**, *1140*, 12−18, https://doi.org/10.1016/j.molstruc.2016.10.057.
47. Ludi, B.; Niederberger, M. Zinc oxide nanoparticles: Chemical mechanisms and classical and non-classical crystallization. *Dalton Trans*. **2013**, *42*, 12554−12568, https://doi.org/10.1039/C3DT50610J.

48. Zare, M.; Namratha, K.; Byrappa, K.; Surendra, D.M.; Yallappa, S.; Hungund, B. Surfactant assisted solvothermal synthesis of ZnO nanoparticles and study of their antimicrobial and antioxidant properties. *J. Mater. Sci. Technol.* **2018**, 1059, 1-9, https://doi.org/10.1016/j.jmst.2017.09.014.
49. Wojnarowicz, J.; Chudoba, T.; Gierlotka, S.; Sobczak, K.; Lojkowski, W. Size control of cobalt-doped ZnO nanoparticles obtained in microwave solvothermal synthesis. *Crystals* **2018**, *8*, 179, 1-18, https://doi.org/10.3390/cryst8040179.
50. Wojnarowicz, J.; Chudoba, T.; Koltsov, I.; Gierlotka, S.; Dworakowska, S. Lojkowski, W. Size control mechanism of ZnO nanoparticles obtained in microwave solvothermal synthesis. *Nanotechnol.* **2018**, *29*, 065601, https://doi.org/10.1088/1361-6528/aaa0ef.
51. Wojnarowicz, J.; Opalinska, A.; Chudoba, T.; Gierlotka, S.; Mukhovskyi, R.; Pietrzykowska, E.; Sobczak, K.; Lojkowski, W. Effect of water content in ethylene glycol solvent on the size of ZnO nanoparticles prepared using microwave solvothermal synthesis. *J. Nanomater*. **2016**, 1-15, https://doi.org/10.1155/2016/2789871.
52. Wu, M.-L.; Chen, D.-H.; Huang, T.C. Preparation of Pd/Pt bimetallic nanoparticles in water/AOT/isooctane microemulsion. *J. Colloid and Interface Sci*. **2001**, *243*, 102-108, https://doi.org/10.1006/jcis.2001.7887.
53. Brahma, S.; Jaiswal, P.; Suresh, K.S.; Lo, K.-Y.; Suwas, S.; Shivashankar, S.A. Effect of substrates and surfactants over the evolution of crystallographic texture of nanostructured ZnO thin films deposited through microwave irradiation. *Thin Solid Films* **2015**, *593*, 81–90, https://doi.org/10.1016/j.tsf.2015.09.005.
54. Xin, Z.; Li, L.; Zhang, X.; Zhang, W. Microwave-assisted hydrothermal synthesis of chrysanthemum-like Ag/ZnO prismatic nanorods and their photocatalytic properties with multiple modes for dye degradation and hydrogen production. *RSC Adv*. **2018**, 8, 6027–6038, https://doi.org/10.1039/C7RA12097D.
55. Shen, X.; Sun, J.; Zhu, G.; Ji, Z.; Chen, Z.; Li, N. Morphological syntheses of ZnO nanostructures under microwave irradiation. *J. Mater. Sci*. **2013**, *48*, 2358–2364, https://doi.org/10.1007/s10853-012-7017-7.
56. Razali, R.; Zak, A.K.; Majid, W.H.A.; Darroudi, M. Solvothermal synthesis of microspheres ZnO nanostructures in DEA media. *Ceram. Int.* **2011**, *37*, 3657-3663, https://doi.org/10.1016/j.ceramint.2011.06.026.
57. Idiawati, R.; Mufti, N.; Taufiq, A.; Wisodo, H.; Laila, I.K.R.; Fuad, A. Effect of growth time on the characteristics of ZnO nanorods. IOP Conf. Series: *Mater. Sci. Eng.* **2017**, *202*, 012050, https://doi.org/10.1088/1757-899X/202/1/012050.
58. de Peres, M.L.; Delucis, R.A.; Amico, S.C.; Gatto, D.A. Zinc oxide nanoparticles from microwave-assisted solvothermal process: Photocatalytic performance and use for wood protection against xylophagous fungus. *Nanomater & Nanotechnol*. **2019**, 9, 1–8, https://doi.org/10.1177/1847980419876201.
59. Dimitriev, Y.; Ivanova, Y.; Iordanova, R. History of sol-gel science and technology (review). *J. Univ. Chem. Technol. & Metallu.* **2008**, *43*, 181-192.
60. Parihar, V.; Raja, M.; Paulose, R. A brief review of structural, electrical and electrochemical properties of zinc oxide nanoparticles. *Rev. Adv. Mater. Sci*. **2018**, *53*, 119-130, https://doi.org/10.1515/rams-2018-0009.
61. Catauro, M.; Tranquillo, E.; Poggetto, G.D.; Pasquali, M.; Dell'Era, A.; Cipriotti, S. Influence of the heat treatment on the particles size and on the crystalline phase of TiO_2 synthesized by sol-gel method. *Materials* **2018**, *11*, 2364, https://doi.org/10.3390/ma11122364.
62. Livage, J.; Henry, M.; Sanchez, C. Sol-gel chemistry of transition metal oxides. *Prog. Solid State Chem*. **1988**. *18*, 259–341, https://doi.org/10.1016/0079-6786(88)90005-2.
63. Parashar, M.; Shukla, V.K.; Singh, R. Metal oxides nanoparticles via sol–gel method: a review on synthesis, characterization and applications. *J. Mater. Sci: Mater Electron*, **2020**, *31*, 3729-3749, https://doi.org/10.1007/s10854-020-02994-8.
64. Singh, G.; Singh, S.P. Synthesis of zinc oxide by sol-gel method and to study its structural properties. *AIP Conference Proceedings* **2020**, *2220*, 020184, https://doi.org/10.1063/5.0001593.
65. Chen, X.; Wu, Z.; Liu, D.; Gao, Z. Preparation of ZnO photocatalyst for the efficient and rapid photocatalytic degradation of azo dyes. *Nanoscale Res. Lett*. **2017**, *12*, 1-10, https://doi.org/10.1186/s11671-0711904-4.
66. Shaikh, R.S.; Ravangave, L.S. Effect of reaction time on some characterization of ZnO nanoparticles. *Int. Res. J. Sci. & Eng., Special Issue A2* **2018**, 187-191, ISSN: 2322-0015.
67. Hasnidawani, J.N.; Azlina, H.N.; Norita, H.; Bonnia, N.N.; Ratim, S.; Ali, E.S. Synthesis of ZnO nanostructures using sol-gel method. *Procedia Chem*. **2016**, *19*, 211 – 216, https://doi.org/10.1016/j.proche.2016.03.095.

68. Iwamura, T.; Goto, S.; Sakaguchi, M.; Chujo, Y. Synthesis of submicrometer zinc oxide particles and zinc oxide nanowires using microwave irradiation. *Chem. Lett.* **2016**, *45*, 508–510, https://doi.org/10.1246/cl.160081.
69. Iwamura, T.; Adachi, K.; Chujo, Y. Simple and rapid eco-friendly synthesis of cubic octamethylsilsesquioxane using microwave irradiation. *Chem. Lett.* **2010**, *39*, 354-355, https://doi.org/10.1246/cl.2010.354.
70. Vanaja, A.; Rao, K.S. Effect of solvents on particle structure, morphology and optical properties of zinc oxide nanoparticles. *Int. J. Adv. Mater. Sci. Eng. (IJAMSE)* **2015**, *4*, 1-8, https://doi.org/10.14810/ijamse.2015.4201.
71. Borm, P.J.A.; Robbins, D.; Haubold, S.; Kuhlbusch, T.; Fissan, H.; Donaldson, K.; Schins, R.; Stone, V.; Kreyling, W.; Lademann, J.; Krutmann, J.; Warheit, D.; Oberdorster, E. The potential risk of nanomaterials: A review carried out for ECETOC. *Part. Fibre Toxicol*. **2006**, *3*, 11–45, https://doi.org/10.1186/1743-8977-3-11.
72. Khan, M.F.; Ansari, A.H.; Hameedullah, M.; Ahmad, E.; Husain, F.M.; Zia, Q.; Baig, U.; Zaheer, M.R.; Alam, M.M.; Khan, A.M.; AlOthman, Z.A.; Ahmad, I.; Ashraf, G.M.; Aliev, G. Sol-gel synthesis of thorn-like ZnO nanoparticles endorsing mechanical stirring effect and their antimicrobial activities: Potential role as nano-antibiotics. *Scientific Reports* **2016,** *6*, 1-12, https://doi.org/10.1038/srep27689.
73. Brintha, S.R.; Ajitha, M. Synthesis and characterization of ZnO nanoparticles via aqueous solution, sol-gel and hydrothermal methods. *J. Appl. Chem. (IOSR-JAC)* **2015**, *8*, 66-72.
74. Sayari, A.; EI Mir, L. Structural and characterization of Ni and Al Co-doped ZnO nanopowders synthesized via the sol-gel process. *Kona Powder and Particle Journal* **2016**, *32*, 154-162, https://doi.org/10.14356/kona.2015003
75. Shohany, B.G.; Zak, A.K. Doped ZnO nanostructures with selected elements - Structural, morphology and optical properties: A review. *Ceramics Int*. **2019**, *46*, 5507-5520, https://doi.org/10.1016/j.ceramint.2019.11.051.
76. Yousefi, R.; Zak, A.K.; Jamali-Sheini, F. The effect of group-I elements on the structural and optical properties of ZnO nanoparticles, *Ceramics Int*. **2013**, *39*, 1371–1377, https://doi.org/10.1016/j.ceramint.2012.07.076.
77. Hameed, A.S.H.; Karthikeyan, C.; Sasikumar, S.; Kumar, V.S.; Kumaresan, S.; Ravi, G. Impact of alkaline metal ions Mg^{2+}, Ca^{2+}, Sr^{2+} and Ba^{2+} on the structural, optical, thermal and antibacterial properties of ZnO nanoparticles prepared by the co-precipitation method. *J. Mater. Chem. B* **2013,** *1*, 5950–5962, https://doi.org/10.1039/C3TB21068E.
78. Zak, A.K.; Majid, W.H.A.; Abrishami, M.E.; Yousefi, R.; Parvizi, R. Synthesis, magnetic properties and X-ray analysis of $Zn_{0.97}X_{0.03}O$ nanoparticles (X = Mn, Ni, and Co) using Scherrer and size-strain plot methods. *Solid State Sci.* **2012**, *14*, 488-494, https://doi.org/10.1016/J.solidstatesciences.2012.01.019.
79. Kaur, P.; Kumar, S.; Chen, C.L.; Hsu, Y-Y.; Chan, T-S.; Dong, C-L.; Srivastava, C.; Singh, A.; Rao, S.M. Investigations on structural, magnetic and electronic structure of Gd-doped ZnO nanostructures synthesized using sol–gel technique. *Appl. Phys. A* **2016**, *122*, 161, https://doi.org/10.1007/s00339-016-9707-5.
80. Barreto, G.; Morales, G.; Cañizo, A.; Eyler, N. Microwave assisted synthesis of ZnO tridimensional nanostructures. *Procedia Mater. Sci.* **2015**, *8*, 535 – 540, https://doi.org/10.1016/j.mspro.2015.04.106.
81. Hasanpoor, M.; Aliofkhazraei, M.; Delavari, H. Microwave-assisted synthesis of zinc oxide nanoparticles. *Procedia Mater. Sci*. **2015**, *11*, 320–325, https://doi.org/10.1016/j.mspro.2015.11.101.
82. Byzynski, G.; Pereira, A.P. Volanti, D.P.; Ribeiro, C.; Longo, E. High-performance ultraviolet-visible driven ZnO morphologies photocatalyst obtained by microwave-assisted hydrothermal method. *J. Photochem. & Photobio. A*: Chem. **2018**, *353*, 358-367, https://doi.org/10.1016/j.jphotochem.2017.11.032.
83. Sadhukhan, P.; Kundu, M.; Rana, S.; Kumar, R.; Das, J.; Sil, P.C. Microwave induced synthesis of ZnO nanorods and their efficacy as a drug carrier with profound anticancer and antibacterial properties. *Toxicol Reports* **2019**, *6*, 176-185, https://doi.org/10.1016/j.toxrep.2019.01.006.
84. Markovic, S.; Simatovic, I.S.; Ahmetovic, S.; Veselinovic, L.; Stojadinovic, S.; Rac, V.; Skapin, S.D.; Bogdanovic, D.B.; Castvan, I.J.; Uskokovic, D. Surfactant-assisted microwave processing of ZnO particles: a simple way for designing the surface-to-bulk defect ratio and improving photo(electro)catalytic properties. *RSC Adv*. **2019**, *9*, 17165-17178, https://doi.org/10.1039/C9RA02553G.
85. Thi, V.H.T.; Lee, B-K. Great improvement on tetracycline removal using ZnO rod-activated carbon fiber composite prepared with a facile microwave method. *J. Hazard. Mater.* **2016**, *324*, 329-339, https://doi.org/10.1016/j.jhazmat.2016.10.066.

86. Sun, H.; Sun, L.; Sugiura, T.; White, M.S.; Stadler, P.; Sariciftci, N.S.; Masuhara, A.; Yoshida, T. Microwave-assisted hydrothermal synthesis of structure-controlled ZnO nanocrystals and their properties in dye-sensitized solar cells. *Electrochem*. **2017**, *85*, 253–261, https://doi.org/10.5796/electrochemistry.85.253.
87. Wannapop, S.; Somdee, A.; Thongtem, T.; Thongtem, S. Synthesis of ZnO nanostructures by microwave irradiation for energy conversion material in for dye sensitized solar cells and materials for photocatalytic dye degradation applications. *J. Ceram. Soc. Japan* **2019**, *127*, 428-434, https://doi.org/10.2109/jcersj2.19015.
88. Pulit-Prociak, J.; Banach, M. Effect of process parameters on the size and shape of nano- and micrometric zinc oxide. *Acta Chim. Slov*. **2016**, *63*, 317–322, https://doi.org/10.17344/acsi.2016.2245.
89. Pauzi, N.; Zain, N.M.; Yusof, N.A.A. Microwave-assisted synthesis of ZnO nanoparticles stabilized with Gum Arabic: effect of microwave irradiation time on ZnO nanoparticles size and morphology. *Bullet. Chem. React. Eng. & Catal*. **2019**, *14*, 182-188, https://doi.org/10.9767/bcrec.14.1.3320.182-188.
90. Gray, R.J.; Jaafar, A.H.; Verrelli, E.; Kemp, N.T. Method to reduce the formation of crystallites in ZnO nanorod thin-films grown via ultra-fast microwave heating. *Thin Solid Films* **2018**, *662*, 116-122, https://doi.org/10.1016/j.tsf.2018.07.03.034.
91. Marzouqi, F.A.; Adawi, H.A.; Qi, K.; Liu, S-y.; Kim, Y.; Selvaraj, R. A green approach to the microwave-assisted synthesis of flower-like ZnO nanostructures for reduction of Cr(VI). *Toxicol. Environ. Chem*. **2019**, *101*, 1–12, https://doi.org/10.1080/02772248.2019.1635602.
92. Wasly, H.S.; El-Sadek, M.S.A.; Henini, M. Influence of reaction time and synthesis temperature on physical properties of ZnO nanoparticles synthesized by hydrothermal method. *Appl. Phys. A* **2018**, *124*, 76, https://doi.org/10.1007/s00339-017-1482-4.
93. Bayrami, A.; Ghorbani, E.; Pouran, S.R.; Habibi-Yangjeh, A.; Khataee, A.; Bayrami, M. Enriched zinc oxide nanoparticles by Nasturtium officinale leaf extract: Joint ultrasound-microwave-facilitated synthesis, characterization, and implementation for diabetes control and bacterial inhibition. *Ultrasonics-Sonochemistry* **2019**, *58*, 104613, 1-8, https://doi.org/10.1016/j.ultsonch.2019.104613.
94. Bayrami, A.; Parvinroo, S.; Habibi-Yangjeh, A.; Pouran, S.R. Bio-extract-mediated ZnO nanoparticles: microwave-assisted synthesis, characterization and antidiabetic activity evaluation. Artificial Cells, *Nanomed. & Biotechnol*. **2018**, *46*, 730–739, https://doi.org/10.1080/21691401.2017.1337025.
95. Chae, H.U.; Rana, A.H.S.; Park, Y-J.; Kim, H-S. High-speed growth of ZnO nanorods in preheating condition using microwave-assisted growth method. *J. Nanosci. Nanotechnol.* **2018**, *18*, 2041–2044, https://doi.org/10.1166/jnn.2018.14971.
96. Chauhan, D.S.; Gopal, C.S.A.; Kumar, D.; Mahato, N.; Quraishi, M.A.; Cho, M.H. Microwave induced facile synthesis and characterization of ZnO nanoparticles as efficient antibacterial agents. *Mater. Discovery* **2018**, *11*, 19-25, https://doi.org/10.1016/j.md.2018.05.001.
97. Fang, M.; Liu, Z.W. Controllable size and photoluminescence of ZnO nanorod arrays on Si substrate prepared by microwave-assisted hydrothermal method, *Ceramics Int*. **2017**, *43*, 6955-6962, https://doi.org/10.1016/j.ceramint.2017.02.119.
98. Giridhar, M.; Naik, H.S.B.; Sudhamani, C.N.; Prabakara, M.C.; Kenchappa, R.; Venugopal, N.; Patil, S. Microwave-assisted synthesis of water-soluble styrylpyridine dye-capped zinc oxide nanoparticles for antibacterial applications. *J. Chin. Chem, Soc*. **2019**, 1–8, https://doi.org/10.1002/jccs.201900029.
99. Goswami, S.R.; Singh, M. Microwave-mediated synthesis of zinc oxide nanoparticles: a therapeutic approach against Malassezia species. *The Institution of Engineering and Technology Biotechnology* **2018**, 1-6, https://doi.org/10.1049/iet-nbt.2018.0007.
100. Hirai, Y.; Furukawa, K.; Sun, H.; Matsushima, Y.; Shito, K.; Masuhara, A.; Ono, R.; Shimbori, Y.; Shiroishi, H.; White, M.S.; Yoshida, T. Microwave-assisted hydrothermal synthesis of ZnO and Zn-terephthalate hybrid nanoparticles employing benzene dicarboxylic acids. *Microsyst Technol*. **2017**, 1-10, https://doi.org/10.1007/s00542-017-3392-y.
101. Sooksaen, P.; Chuankrerkkul, N. Morphology-design and semiconducting characteristics of zinc oxide nanostructures under microwave irradiation. *Integrated Ferroelectrics* **2017**, 91-102, https://doi.org/10.1080/10584587.2017.1285194.
102. Jaafar, N.F.; Najman, A.M.M.; Marfura, A.; Jusoh, N.W.C. Strategies for the formation of oxygen vacancies in zinc oxide nanoparticles used for photocatalytic degradation of phenol under visible light irradiation. *J. Photochem. & Photobio A: Chem.* **2019**, *388*, 112202, 1-10, https://doi.org/10.1016/j.jphotochem.2019.112202.

103. Malik, L.A.; Bashir, A.; Manzoor, T.; Pandith, A.H. Microwave-assisted synthesis of glutathione-coated hollow zinc oxide for the removal of heavy metal ions from aqueous systems. *RSC Adv*. **2019**, *9*, 15976 – 15985, https://doi.org/10.1039/C9RA00243.
104. Al-Sabahi, J.; Bora, T.; Al-Abri, M.; Dutta, J. Controlled defects of zinc oxide nanorods for efficient visible light photocatalytic degradation of phenol. *Mater.* **2016**, *9*, 238, 1-10, https://doi.org/10.3390/ma9040238.
105. Pimentel, A.; Ferreira, S.H.; Nunes, D.; Calmeiro, T.; Martins, R.; Fortunato, E. Microwave synthesized ZnO nanorod arrays for UV sensors: A seed layer annealing temperature study. *Mater.* **2016**, *9*, 299, 1-15, https://doi.org/10.3390/ma9040299.
106. Tan, S.T.; Tan, C.H.; Chong, W.Y.; Yap, C.C.; Umar, A.A.; Ginting, R.T.; Lee, H.B.; Lim, K.S.; Yahaya, M.; Salleh, M.M. Microwave-assisted hydrolysis preparation of highly crystalline ZnO nanorod array for room temperature photoluminescence-base CO gas sensor. *Sensors and Actuators B* **2016**, *227*, 304–312, https://doi.org/10.1016/j.snb.2015.12.058
107. Song, H.; Zhu, K.; Liu, Y.; Zhai, X. Microwave-assisted synthesis of ZnO and its photocatalytic activity in degradation of CTAB. *Rus. J. Phys. Chem. A* **2017**, *91*, 59–62, https://doi.org/10.1134/S003602441701.
108. Nandi, A.; Nag, P.; Saha, H.; Majumdar, S. Precursor dependent morphologies of microwave assisted ZnO nanostructures and their VOC detection properties. *Mater. Today: Proceedings* **2018**, *5*, 9831-9838, https://doi.org/10.1016/j.matpr.2017.10.174.
109. Papadaki, D.; Foteinis, S.; Mhlongo, G.H.; Nkosi, S.S.; Motaung, D.E.; Ray, S.S.; Tsoutsos, T.; Kiriakidis, G. Life cycle assessment of facile microwave-assisted zinc oxide (ZnO) nanostructures. *Sci. Tot. Environ*. **2017**, *586*, 566-575, https://doi.org/10.1016/j.scitotenv.2017.02.019.
110. Quirino, M.R.; Oliveira, M.J.C.; Keyson, D.; Lucena, G.L.; Oliveira, J.B.L.; Gama, L. Synthesis of zinc oxide by microwave hydrothermal method for application to transesterification of soyabean oil (biodiesel). *Mater. Chem. Phys.* **2016**, *185*, 24-30, https://doi.org/10.1016/j.matchemphys.2016.09.06.
111. Witkowski, B.S.; Dluzewski, P.; Kaszewski, J.; Sylwia, L.W. Ultra-fast epitaxial growth of ZnO nano/microrods on a GaN substrate, using the microwave-assisted hydrothermal method. *Mater. Chem. Phys*. **2018**, *205*, 16-22, https://doi.org/10.1016/j.matchemphys.2017.11.00.
112. Thankachan, R.M.; Joy, N.; Abraham, J.; Kalarikkal, N.; Thomas, S.; Oluwafemi, O.S. Enhanced photocatalytic performance of ZnO nanostructures produced via a quick microwave assisted route for the degradation of rhodamine in aqueous solution. *Mater. Res. Bull.* **2017**, *85*, 131-139, https://doi.org/10.1016/j.materresbull.2016.09.009.
113. Husham, M.; Hamidon, M.N.; Paiman, S.; Abuelsamen, A.A.; Farhat, O.F.; Al-Dulaimi, A.A. Synthesis of ZnO nanorods by microwave-assisted chemical-bath deposition for highly sensitive self-powered UV detection application. *Sensors and Actuators A* **2017**, *263*, 166-173, https://doi.org/10.1016/j.sna.2017.05.041.
114. Salah, N.; AL-Shawafi, W.M.; Alshahrie, A.; Baghdadi, N.; Soliman, Y.M.; Memic, A. Size controlled, antimicrobial ZnO nanostructures produced by the microwave assisted route. *Mater. Sci. & Eng. C* **2019**, *99*, 1164–1173, https://doi.org/10.1016/j.msec.2019.02.077.
115. Sakata, K.; Macounová, K.M., Nebel, R.; Krtil, P. pH dependent ZnO nanostructures synthesized by hydrothermal approach and surface sensitivity of their photoelectrochemical behaviour. *SN Appl. Sci*. **2020**, *2*, 203, 1-8, https://doi.org/10.1007/s42452-020-1975-1.
116. Sekhar, M.C.; Ramana, M.V. Instant synthesis of ZnO nanoparticles by microwave hydrothermal method. *Int. J. NanoSci. Nanotechnol*. **2017**, *8*, 17-23, ISSN: 0974-3081.
117. Šarić, A.; Despotović, I.; Štefanić, G. Alcoholic solvent influence on ZnO synthesis: A joint experimental and theoretical study. *J. Phys. Chem. C* **2019**, 123, 29394−2940, https://doi.org/10.1021/acs.jpcc.9b07411.
118. Ahammed, K.R.; Ashaduzzaman, M.; Paul, S.C.; Nath, M.R.; Bhowmik, S.; Saha, O.; Rahaman, M.M.; Bhowmik, S.; Aka, T.D. Microwave assisted synthesis of zinc oxide (ZnO) nanoparticles in a noble approach: utilization for antibacterial and photocatalytic activity. *SN Appl. Sci.* **2020,** *2*, 955, 1-14, https://doi.org/10.1007/s42452-020-2762-8.
119. Xiangyang, B.; Linlin, L.; Huiyu, L.; Longfei, T.; Tianlong, L.; Xianwei, M. Small molecule ligand solvothermal synthesis of ZnO nanoparticles and anti-infection application in vivo. *ACS Appl. Mater. Interfaces* **2015**, *7*, 1308-1317, https://doi.org/10.1021/am507532p.
120. Angaiah, S.; Arunachalam, S.; Murugadoss, V.; Vijayakumar, G. A Facile Polyvinylpyrrolidone assisted solvothermal synthesis of zinc oxide nanowires and nanoparticles and their influence on the photovoltaic performance of dye sensitized solar cell. *ES Energy Environ*. **2019**, *4*, 59–65, https://doi.org/10.30919/esee8c280.

121. Feng, W.; Huang, P.; Wang, B.; Wang, C.; Wang, W.; Wang, T.; Chen, S.; Lv, R.; Qin, Y.; Ma, J. Solvothermal synthesis of ZnO with different morphologies in dimethylacetanamide media. *Ceramics Int*. **2015,** *42*, 2250-2256, https://doi.org/10.1016/j.ceramint.2015.10.018.
122. Mao, Y.; Li, Y.; Zou, Y.; Shen, X.; Zhu, L.; Liao, G. Solvothermal synthesis and photocatalytic properties of ZnO micro/nanostructures. *Ceramics Int.* **2018**, *45*, 1724-1729, https://doi.org/10.1016/j.ceramint.2018.10.054.
123. Wojnarowicz, J.; Chudoba, T.; Gierlotka, S.; Lojkowski, W. Effect of microwave radiation power on the size of aggregates of ZnO NPs prepared using microwave solvothermal synthesis. *Nanomater*. **2018**, *8*, 343, 1-17, https://doi.org/10.3390/nano8050343.
124. Nuraqeelah, M.S.; Wee, B.S.; Chin, S.F.; Kok, K.Y. Synthesis and characterization of zinc oxide nanoparticles with small particle size distribution. *Acta Chim. Slov*. **2018**, *65*, 578–585, https://doi.org/10.17344/acsi.2018.4213.
125. Yao, Q.; Wang, C.; Fan, B.; Wang, H.; Sun, Q.; Jin, C.; Zhang, H. One-step solvothermal deposition of ZnO nanorod arrays on a wood surface for robust superamphiphobic performance and superior ultraviolet resistance. *Scientific Reports* **2016**, *6*, 35505, 1-11, https://doi.org/10.1038/srep35505.
126. Bhatta, L.K.G.; Bhatta, U.M.; Venkatesh, K. Facile microwave-assisted synthesis of zinc oxide and characterization. *J. Scienti. Industr. Res*. **2019**, *78*, 173-176, ISSN: 0975-1084.
127. Jamatia, T.; Skoda, D.; Urbanek, P.; Munster, L.; Sevcik, J.; Kuritka, I. Microwave-assisted particle size-controlled synthesis of ZnO nanoparticles and its application in fabrication of PLED device. Applied Nanotechnology and Nanoscience International Conference (ANNIC 2018), IOP Conf. Series: *J. Phys: Conf. Series*, 1310 **2019**, 012012, https://doi.org/10.1088/1742-6596/1310/1/012012.
128. Karthikeyan, L.; Akshaya, M.V.; Basu, P.K. Microwave assisted synthesis of ZnO and Pd-ZnO nanospheres for UV photodetector. *Sensors and Actuators A: Physical* **2017**, 264, 90-95, https://doi.org/10.1016/j.sna.2017.06.013.
129. Kumar, V.; Gohain, M.; Som, S.; Kumar, V.; Bezuindenhoudt, B.C.B.; Swart, H.C. Microwave assisted synthesis of ZnO nanoparticles for lighting and dye removal application. *Physica B: Condensed Matter* **2016**, *480*, 36-41, https://doi.org/10.1016/j.physb.2015.07.020.
130. Pimentel, A.; Rodrigues, J.; Duarte, P.; Nunes, D.; Costa, F.M.; Monteiro, T.; Martins, R.; Fortunato, E. Effect of solvents on ZnO nanostructures synthesized by solvothermal method assisted by microwave radiation: a photocatalytic study. *J. Mater. Sci.* **2015**, *50*, 5777-5787, https://doi.org/10.1007/s10853-015-9125-7.
131. Saloga, P.E.J.; Thünemann, A.F. Microwave-assisted synthesis of ultrasmall zinc oxide nanoparticles. *Langmuir* **2019**, *35*, 12469−12482, https://doi.org/10.1021/acs.langmuir.9b01921.
132. Skoda, D.; Urbanek, P.; Sevcik, J.; Munster, L.; Antos, J.; Kuritka, I. Microwave-assisted synthesis of colloidal ZnO nanocrystals and their utilization in improving polymer light emitting diodes efficiency. *Mater. Sci. Eng. B* **2018**, *232*, 22-32, https://doi.org/10.1016/j.mseb.2018.10.013.
133. Ikono, R.; Akwalia, P.R.; Siswanto, Wahyu, B.W.; Sukarto, A.; Rochman, N.T. Effect of pH variation on particle size and purity of nano zinc oxide synthesized by sol-gel method. *Int. J. Eng. & Technol. (IJET-IJENS)* **2012**, *12*, 5-9.
134. Divya, B.; Karthikeyan, C.; Rajasimman, M. Chemical synthesis of zinc oxide nanoparticles and its application of dye decolourization. *Int. J. Nanosci. Nanotechnol*. **2018**, *14*, 267-275.
135. Prasad, T.; Halder, S.; Goyat, M.S.; Dhar, S.S. Morphological dissimilarities of ZnO nanoparticles and its effect on thermo-physical behavior of epoxy composites. *Polymer Composites* **2018**, *39*, 135-145, https://doi.org/10.1002/pc.23914.
136. Ashraf, R., Riaz, S., Khaleeq-ur-Rehman, M., and Naseem, S. (**2013**). Synthesis and characterization of ZnO nanoparticles. The 2013 World Congress on Advances in Nano, Biomechanics, Robotics and Energy Research (ANBRE13), Seoul, Korea, August, 25-28, 2013.
137. Muñoz-Fernandez, L.; Sierra-Fernandez, A.; Miloševic, O.; Rabanal, M.E. Solvothermal synthesis of Ag/ZnO and Pt/ZnO nanocomposites and comparison of their photocatalytic behaviors on dyes degradation. *Adv. Powd. Technol.* **2016**, *27*, 983-993, https://doi.org/10.1016/j.apt.2016.03.021.
138. Vakili, B.; Shahmoradi, B.; Maleki, A.; Safari, M.; Yang, J.; Pawar, R.R.; Lee, S-M. Synthesis of immobilized cerium doped ZnO nanoparticles through the mild hydrothermal approach and their application in the photodegradation of synthetic wastewater. *J. Mol. Liq.* **2018**, *280*, 230-237, https://doi.org/10.1016/j.molliq.2018.12.103.

139. Gupta, R.; Eswar, N.K.; Modak, J.M.; Madras, G. Effect of morphology of zinc oxide in ZnO-CdS-Ag tenary nanocomposite towards photocatalytic inactivation of *E. coli* under UV and visible light. *Chem. Eng. J*. **2017**, *307*, 966-980, https://doi.org/10.1016/j.cej.2016.08.142.
140. Yuvaraj, S.; Fernandez, A.C.; Sundararajan, M.; Dash, C.S.; Sakthivel, P. Hydrothermal synthesis of ZnO–CdS nanocomposites: Structural, optical and electrical behaviour. *Ceramics Int.* **2020**, *46*, 391-402, https://doi.org/10.1016/j.ceramint.2019.08.274.
141. Manavalan, S.; Veerakumar, P.; Chen, S-M.; Lin, K-C. Three-dimensional zinc oxide nanostars anchored on graphene oxide for voltammetric determination of methyl parathion. *Microchimica Acta* **2020**, *187*, 1-13, https://doi.org/10.1007/s00604-019-4031-3.
142. Rakkesh, R.A.; Durgalakshmi, D.; Karthe, P.; Balakumar, S. Anisotropic growth and strain-induced tunable optical properties of Ag–ZnO hierarchical nanostructures by a microwave synthesis method. *Mater. Chem. Phys.* **2020**, 244, 122720, https://doi.org/10.1016/j.matchemphys.2020.122720.
143. Xin, Z.; Li, L.; Zhang, X.; Zhang, W. Microwave-assisted hydrothermal synthesis of chrysanthemum-like Ag/ZnO prismatic nanorods and their photocatalytic properties with multiple modes for dye degradation and hydrogen production. *RSC Adv*. **2018**, 8, 6027, https://doi.org/10.1039/C7RA12097D.
144. Sankar ganesh, R.; Navaneethan, M.; Mani, G.K.; Ponnusamy, S.; Tsuchiya, K.; Muthamizhchelvan, C.; Kawasaki, S.; Hayahawa, Y. Influence of Al doping on structural, morphological, optical and gas sensing properties of ZnO nanorods. *J. Alloys & Compounds* **2017**, *698*, 555-564, https://doi.org/10.1016/j.jallcom.2016.12.187.
145. Gabriela, B.; Camila, M.; Volanti, D.P.; Ferrer, M.M.; Gouveia, A.F.; Cauê, R.; Juan, A.; Elson, L. The interplay between morphology and photocatalytic activity in ZnO and N-doped ZnO crystals. *Mater. & Design* **2017**, *120*, 363-375, https://doi.org/10.1016/j.matdes.2017.02.020.
146. Wojnarowicz, J.; Omelchenko, M.; Szczytko, J.; Chudoba, T.; Gierlotka, S.; Majhofer, A.; Twardowski, A.; Lojkowski, W. Structural and magnetic properties of Co-Mn codoped ZnO nanoparticles obtained by microwave solvothermal synthesis. *Crystals* **2018**, *8*, 410, https://doi.org/10.3390/cryst8110410.
147. Gao, X.; Zhang, T.; Wu, Y.; Yang, G.; Tan, M.; Li, X.; Xie, H.; Pan, J.; Tan, Y. Isobutanol synthesis from syngas on Zn-Cr based catalysts: New insights into the effect of morphology and facet of ZnO nanocrystal. *Fuel* **2018**, *217*, 21-30, https://doi.org/10.1016/j.fuel.2017.12.065.
148. Aksoy, S.; Caglar, Y. Synthesis of Mn doped ZnO nanopowders by MW-HTS and its structural, morphological and optical characteristics. *J. Alloys and Compounds* **2019**, *781*, 929-935, https://doi.org/10.1016/j.jallcom.2018.12.101.
149. Wojnarowicz, J.; Mukhovskyi, R.; Pietrzykowska, E.; Kusnieruk, S.; Mizeracki, J.; Lojkowski, W. Microwave solvothermal synthesis and characterization of manganese-doped ZnO nanoparticles. *Beilstein J. Nanotechnol*. **2016**, *7*, 721–732, https://doi.org/10.3762/bjnano.7.64.
150. Guruvammal, D.; Selvaraj, S.; Sundar, S.M. Structural, optical and magnetic properties of Co doped ZnO DMS nanoparticles by microwave irradiation method. *J. Magnetism and Magnetic Mater.* **2018,** *452*, 335-342, https://doi.org/10.1016/j.jmmm.2017.12.097.
151. Jayathilake, D.S.Y.; Peiris, T.A.N.; Sagu, J.S.; Potter, D.B.; Wijayantha, K.G.U.; Carmalt, C.J.; Southee, D.J. Microwave-assisted synthesis and processing of Al-doped, Ga-doped, and Al, Ga-codoped ZnO for the pursuit of optimal conductivity for transparent conducting film fabrication. *ACS Sustainable Chem. Eng*. **2017**, *5*, 4820−4829, https://doi.org/10.1021/acssuschemeng.7b00263.
152. Kadam, A.N.; Kim, T.G.; Shin, D-S.; Garadkar, K.M.; Park, J. Morphological evolution of Cu doped ZnO for enhancement of photocatalytic activity. *J. Alloys and Compounds* **2017**, *710*, 102-113, https://doi.org/10.1016/j.jallcom.2017.03.150.
153. Liu, K.; Qin, Y.; Muhammad, Y.; Zhu, Y.; Tang, R.; Chen, N.; Shi, H.; Zhang, H.; Tong, Z.; Yu, B. Effect of Fe_3O_4 content and microwave reaction time on the properties of Fe_3O_4/ZnO magnetic nanoparticles. *J. Alloys and Compounds* **2019**, *781*, 790-799, https://doi.org/10.1016/j.jallcom.2018.12.085.
154. Meng, Q.; Cui, J.; Tang, Y.; Han, Z.; Zhao, K.; Zhang, G.; Diao, Q. Solvothermal synthesis of dual-porous CeO_2-ZnO composite and its enhanced acetone sensing performance. *Ceramics Int*. **2019**, *45*, 4103-4107, https://doi.org/10.1016/j.ceramint.2018.10.239.
155. Neupane, G.R.; Kaphle, A.; Hari, P. Microwave-assisted Fe-doped ZnO nanoparticles for enhancement of silicon solar cell efficiency. *Solar Energy Materials and Solar Cells* **2019**, *201*, 110073, https://doi.org/10.1016/j.solmat2019.110073.

156. Rosowska, J.; Kaszewski, J.; Witkowski, B.; Wachnicki, Ł.; Kuryliszyn-Kudelska, I.; Godlewski, M. The effect of iron content on properties of ZnO nanoparticles prepared by microwave hydrothermal method. *Optical Mater*. **2020**, *109*, 110089, https://doi.org/10.1016/j.optmat.2020.110089.
157. Das, S.; Das, S.; Sutradhar, S. Effect of Gd^{3+} and Al^{3+} on optical and dielectric properties of ZnO nanoparticle prepared by two-step hydrothermal method. *Ceramics Int*. **2017**, *43*, 6932-6941, https://doi.org/10.1016/j.ceramint.2017.02.116.
158. Vinoditha, U.; Sarojini, B.K.; Sandeep, K.M.; Narayana, B.; Maidur, S.R.; Patil, P.S.; Balakrishna, K.M. Defects-induced nonlinear saturable absorption mechanism in europium-doped ZnO nanoparticles synthesized by facile hydrothermal method. *Appl. Phys. A* **2019**, *125*, 1-11, https://doi.org/10.1007/s00339-019-2732-4.
159. Lin, L-Y.; Kavadiya, S.; Karakocak, B.B.; Nie, Y.; Raliya, R.; Wang, S.T.; Berezin, M.Y.; Biswas, P. ZnO_{1-x}/carbon dots composite hollow spheres: Facile aerosol synthesis and superior CO_2 photoreduction under UV, visible and near-infrared irradiation. *Appl. Cataly. B: Environ*. **2018**, *230*, 36–48, https://doi.org/10.1016/j.apcatb.2018.02.018.
160. Obaidullah, Md.; Furusawa, T.; Siddiquey, I.A.; Sato, M.; Suzuki, N. Synthesis of ZnO-Al_2O_3 core-shell nanocomposite materials by fast and facile microwave irradiation method and investigation of their optical properties. *Adv. Powder. Technol*. **2017**, *28*, 2678-2686, https://doi.org/10.1016/j.apt.2017.07.020.